

A theoretical framework of BL Her stars. I. Effect of metallicity and convection parameters on period-luminosity and period-radius relations

Susmita Das^{1*}, Shashi M. Kanbur², Radoslaw Smolec³, Anupam Bhardwaj⁴,
Harinder P. Singh¹ and Marina Rejkuba⁵

1. Department of Physics & Astrophysics, University of Delhi, Delhi 110007, India

2. Department of Physics, State University of New York Oswego, Oswego, NY 13126, USA

3. Nicolaus Copernicus Astronomical Center of the Polish Academy of Sciences, Bartycka 18, PL-00-716 Warszawa, Poland

4. Kavli Institute for Astronomy and Astrophysics, Peking University, Yi He Yuan Lu 5, Hai Dian District, Beijing 100871, China

5. European Southern Observatory, Karl-Schwarzschild-StraÙe 2, D-85748 Garching bei München, Germany

Accepted 2020 November 23. Received 2020 November 19; in original form 2020 September 10

ABSTRACT

We present a new grid of convective BL Herculis models using the state-of-the-art 1D non-linear radial stellar pulsation tool MESA-RSP. We investigate the impact of metallicity and four sets of different convection parameters on multi-wavelength properties. Non-linear models were computed for periods typical for BL Her stars, i.e. $1 \leq P(\text{days}) \leq 4$ covering a wide range of input parameters - metallicity ($-2.0 \text{ dex} \leq [\text{Fe}/\text{H}] \leq 0.0 \text{ dex}$), stellar mass ($0.5M_{\odot}$ - $0.8M_{\odot}$), luminosity ($50L_{\odot}$ - $300L_{\odot}$) and effective temperature (full extent of the instability strip; in steps of 50K). The total number of BL Her models with full-amplitude stable pulsations used in this study is 10280 across the four sets of convection parameters. We obtain their multiband ($UBVRIJHKLL'M$) light curves and derive new theoretical period-luminosity (PL), period-Wesenheit (PW) and period-radius (PR) relations at mean light. We find that the models computed with radiative cooling show statistically similar slopes for PL , PW and PR relations. Most empirical relations match well with the theoretical PL , PW and PR relations from the BL Her models computed using the four sets of convection parameters. However, PL slopes of the models with radiative cooling provide a better match to empirical relations for BL Her stars in the LMC in the HK_S bands. For each set of convection parameters, the effect of metallicity is significant in U and B -bands and negligible in infrared bands, which is consistent with empirical results. No significant metallicity effects are seen in the PR relations.

Key words: hydrodynamics-methods: numerical- stars: oscillations (including pulsations)- stars: Population II- stars: variables: Cepheids- stars: low-mass

1 INTRODUCTION

Type II Cepheids (T2Cs) are pulsating stars located in the instability strip of the Hertzsprung-Russell diagram (HRD). T2Cs are brighter than the RR Lyrae stars but fainter than the classical Cepheids. Based on their pulsational period, T2Cs are divided into the following subclasses: the BL Herculis (BL Her: $1 \leq P(\text{days}) \leq 4$), the W Virginis (W Vir: $4 \leq P(\text{days}) \leq 20$) and the RV Tauris (RV Tau: $P \geq 20$ days) (Soszyński et al. 2018). However, the period separation for different subclasses is not strict, for example, the upper limit on the period of BL Her stars is set at 4 days in the Magellanic Clouds Soszyński et al. (2018) and 5 days in the Galactic bulge Soszyński et al. (2017). Similar to RR Lyrae stars and classical Cepheids, T2Cs follow well-defined period-luminosity (PL) relationships (Matsunaga et al. 2006; Groenewegen et al. 2008; Matsunaga et al. 2009; Ciechanowska et al. 2010; Matsunaga et al. 2011; Ripepi et al. 2015; Bhardwaj et al. 2017a,b; Groenewegen & Jurkovic 2017b; Braga et al. 2018), which makes

them useful distance indicators (see reviews, Beaton et al. 2018; Bhardwaj 2020).

T2Cs are population II stars and trace low mass, metal-poor, old-age stellar populations. However, recent studies suggest that W Vir stars may have their origin in binary systems (Groenewegen & Jurkovic 2017a) and that RV Tau stars may also have massive and younger progenitors (Manick et al. 2018). T2Cs have a wide range of metallicities (Welch 2012). While Clement et al. (2001) noted that all the Galactic Globular Clusters (GGCs) containing T2Cs have $[\text{Fe}/\text{H}] < -1.0$ dex, Galactic field T2Cs were found to have metallicities in the range $-1.0 \text{ dex} < [\text{Fe}/\text{H}] < 0 \text{ dex}$ (Schmidt et al. 2011). T2Cs in the Bulge have photometric metallicities ranging from -1.4 dex to $+0.6 \text{ dex}$, with $[\text{Fe}/\text{H}]_{\text{mean}} = -0.6 \pm 0.17 \text{ dex}$ (Harris & Wallerstein 1984; Wallerstein 2002). In a recent study to understand the origin of the Galactic Halo, Wallerstein & Farrell (2018) found $[\text{Fe}/\text{H}] > -0.9 \text{ dex}$ for a majority of the field T2Cs. We therefore adopt a broad range of metallicities, $-2 \text{ dex} < [\text{Fe}/\text{H}] < 0 \text{ dex}$ for computing BL Her models in the present study.

Empirical PL relations of T2Cs have been studied extensively

* E-mail: susmitadas130@gmail.com

in the last few decades. [Nemec et al. \(1994\)](#) provided $P - L - [\text{Fe}/\text{H}]$ relations for T2Cs in the GGCs in the optical BV bands. [Matsunaga et al. \(2006\)](#) did not find any significant metallicity effect on the PL relations in their study of PL relations using 46 T2Cs in 26 GGCs; the observations were obtained from the Infrared Survey Facility (IRSF) 1.4-m telescope in the near-infrared JHK_S bands. Using 39 T2Cs in the Galactic Bulge monitored with the SOFI infrared camera on the 3.5-m NTT on ESO/La Silla, [Groenewegen et al. \(2008\)](#) provided PL relations in the K -band and estimated a distance modulus of $14.51 \pm 0.12 \pm 0.07$ (systematic) mag to the Galactic Centre. The PL relations for Galactic T2Cs in the Gaia G -band have been provided by [Clementini et al. \(2016\)](#). In a series of papers, [Matsunaga et al. \(2009, 2011\)](#) presented near-infrared (JHK_S) PL and Wesenheit relations for T2Cs in the Large (LMC) and Small (SMC) Magellanic Clouds obtained using data from IRSF and SIR-IUS. Near-infrared PL and period-Wesenheit (PW) relations for T2Cs in the LMC have been presented by [Ripepi et al. \(2015\)](#) using the VISTA Magellanic Cloud survey (VMC, [Cioni et al. 2011](#)) and by [Bhardwaj et al. \(2017a\)](#) using observations obtained by the Large Magellanic Cloud Near-infrared Synoptic Survey (LMC-NISS, [Macri et al. 2015](#)). Recently, [Manick et al. \(2017\)](#) published PW relations for T2Cs in the LMC using the Optical Gravitational Lensing Experiment (OGLE-III, [Soszyński et al. 2008](#)) data, while [Groenewegen & Jurkovic \(2017b\)](#) presented PL relations of the Magellanic Cloud T2Cs based on OGLE-III data reporting no dependence on metallicity.

[Burki & Meylan \(1986\)](#) and [Balog et al. \(1997\)](#) are few of the earlier studies where the empirical period-radius (PR) relations of T2Cs were investigated. A detailed study of the PR relations of T2Cs in the Magellanic Clouds has been carried out by [Groenewegen & Jurkovic \(2017b\)](#) based on OGLE-III data. They found the PR relations to have little or no dependence on metallicity.

On the theoretical front, several linear and non-linear convective T2C models, in particular, BL Her models have been computed by [Bono et al. \(1995, 1997a,b\)](#); [Marconi & Di Criscienzo \(2007\)](#); [Smolec et al. \(2012\)](#); [Smolec & Moskalik \(2012, 2014\)](#); [Smolec \(2016\)](#). [Buchler & Moskalik \(1992\)](#) had predicted period doubling in BL Her stars which is caused by the 3:2 resonance between the fundamental mode and the first overtone. This was confirmed almost 20 years later when the period doubling behaviour was observed in a 2.4-d BL Her type variable in the Galactic bulge and consistently modeled with the observed light curves ([Soszyński et al. 2011](#); [Smolec et al. 2012](#)). Few theoretical studies have provided PL and PR relations for BL Her models. Theoretical near-infrared period-magnitude and PW relations for BL Her models in the metal abundance range of $Z = 0.0001$ to $Z = 0.004$ ¹ were derived by [Di Criscienzo et al. \(2007\)](#) while [Marconi & Di Criscienzo \(2007\)](#) presented theoretical PR relation for BL Her models and found it to be in excellent agreement with the empirical relation from [Burki & Meylan \(1986\)](#).

The recently released non-linear Radial Stellar Pulsation (RSP) tool in *Modules for Experiments in Stellar Astrophysics* (MESA, [Paxton et al. 2011, 2013, 2015, 2018, 2019](#)) may be used for generating multi-wavelength light curves of classical pulsators. Along with being an open-source code, MESA-RSP offers the advantage of testing how properties of the models depend on the details of convection model used, by varying convective parameters. [Das et al. \(2020\)](#) computed a few RR Lyrae, BL Her and classical Cepheid models using MESA-RSP and found the theoretical period-colour (PC) relations

to be in good agreement with the empirical PC relations. The aim of this project is to compute a very fine grid of BL Her models, encompassing a wide range of metallicity, mass, luminosity and effective temperature using the most recent, state-of-the-art stellar pulsation code, the MESA-RSP. We also obtain theoretical PL and PR relations for these stars and test the effect of convection parameters and metallicity on these relations. The reason for choosing BL Her stars only (and not the other subclasses of T2Cs) for our study is two-fold: (i) [Matsunaga et al. \(2011\)](#) found evidence that PL relations of BL Her and W Vir stars should be discussed independently (ii) The highly non-adiabatic longer-period T2Cs (W Vir and RV Tau stars) pose problems for the existing pulsation codes and are current limitations of MESA-RSP ([Smolec 2016](#); [Paxton et al. 2019](#)). However, MESA-RSP may be reliably used for modelling the shortest-period class of T2Cs, the BL Her stars.

The structure of this paper is as follows: The BL Her models computed using MESA-RSP are described in Section 2. In Sections 3 and 4, we study the PL and PR relations of these models and investigate any possible dependence of these relations on metallicity and convection parameters. Finally, we summarise the results of this study in Section 6.

2 THE STELLAR PULSATION MODELS

Since MESA-RSP offers the possibility of using different convection parameter sets, we explore the effect of different convection parameters on the multi-wavelength PL and PR relations of a finely computed grid of BL Her models. We note here that MESA-RSP uses the theory of turbulent convection as outlined in [Kuhfuss \(1986\)](#) and follows [Smolec & Moskalik \(2008\)](#) in its treatment of stellar pulsation. The free parameters that enter the convective model are provided in Tables 3 and 4 of [Paxton et al. \(2019\)](#). For convenience, they are listed in Table 1. Set A corresponds to the simplest convection model, set B adds radiative cooling, set C adds turbulent pressure and turbulent flux, and set D includes these effects simultaneously. A detailed description of the free parameters and their standard values is provided in [Smolec & Moskalik \(2008\)](#). In brief, parameters α_p and α_c were introduced by [Yecko et al. \(1998\)](#) and their values were set at $\alpha_p=2/3$ and $\alpha_c=\alpha_s$. The value for $\gamma_r=2\sqrt{3}$ is obtained from [Wuchterl & Feuchtinger \(1998\)](#). Neglecting radiative cooling and turbulent pressure reduces the time-independent version of the convection model ([Kuhfuss 1986](#)) to the standard mixing-length theory (MLT), provided the values for α_s , α_c and α_d are kept the same as in Table 1. [Paxton et al. \(2019\)](#) suggest $\alpha_t \approx 0.01$, $\alpha_m \lesssim 1$, and $\alpha \lesssim 2$ as useful starting choices. We stress here that we have not made any changes to the free parameters in this work and have used the four sets of convection parameters as provided in [Paxton et al. \(2019\)](#). We use MESA r11701 for our present study. OPAL opacity tables ([Iglesias & Rogers 1996](#)) supplemented at low temperatures with [Ferguson et al. \(2005\)](#) opacity data were adopted.

2.1 Linear computations

We compute a fine grid of BL Her models for each of the four convection sets with the following input parameters:

- (i) Metallicity (Corresponding ZX values are provided in Table 2)

$$[\text{Fe}/\text{H}] \text{ (in dex)} = -2, -1.5, -1.35, -1, -0.5, -0.2, 0$$

- (ii) Stellar mass (M)

¹ Equivalent metallicity range, $-2.62 \text{ dex} \leq [\text{Fe}/\text{H}] \leq -0.66 \text{ dex}$

Table 1. The free parameters and their associated values in the convective parameter sets A, B, C and D of the MESA-RSP convection model.

Name	Parameter description	Set A	Set B	Set C	Set D
α	Mixing-length parameter	1.5	1.5	1.5	1.5
α_m	Eddy-viscous dissipation parameter	0.25	0.50	0.40	0.70
α_s	Turbulent source parameter	$\frac{1}{2} \sqrt{\frac{1}{3}}$	$\frac{1}{2} \sqrt{\frac{1}{3}}$	$\frac{1}{2} \sqrt{\frac{1}{3}}$	$\frac{1}{2} \sqrt{\frac{1}{3}}$
α_c	Convective flux parameter	$\frac{1}{2} \sqrt{\frac{1}{3}}$	$\frac{1}{2} \sqrt{\frac{1}{3}}$	$\frac{1}{2} \sqrt{\frac{1}{3}}$	$\frac{1}{2} \sqrt{\frac{1}{3}}$
α_d	Turbulent dissipation parameter	$\frac{3}{8} \sqrt{\frac{1}{3}}$	$\frac{3}{8} \sqrt{\frac{1}{3}}$	$\frac{3}{8} \sqrt{\frac{1}{3}}$	$\frac{3}{8} \sqrt{\frac{1}{3}}$
α_p	Turbulent pressure parameter	0	0	0	0
α_t	Turbulent flux parameter	0	0	0.01	0.01
γ_r	Radiative cooling parameter	0	$2\sqrt{3}$	0	$2\sqrt{3}$

Table 2. Chemical compositions of the adopted pulsation models*.

[Fe/H]	Z	X
-2.00	0.00014	0.75115
-1.50	0.00043	0.75041
-1.35	0.00061	0.74996
-1.00	0.00135	0.74806
-0.50	0.00424	0.74073
-0.20	0.00834	0.73032
0.00	0.01300	0.71847

* The Z and X values are estimated from the [Fe/H] values by assuming the primordial helium value of 0.2485 from the WMAP CMB observations (Hinshaw et al. 2013) and the helium enrichment parameter value of 1.54 (Asplund et al. 2009). The solar mixture is adopted from Asplund et al. (2009).

- (a) Low-mass range = $0.5M_{\odot}$, $0.55M_{\odot}$, $0.6M_{\odot}$
- (b) High-mass range = $0.65M_{\odot}$, $0.7M_{\odot}$, $0.75M_{\odot}$, $0.8M_{\odot}$
- (iii) Stellar luminosity (L)
 - (a) For low-mass range = $50L_{\odot}$ to $200L_{\odot}$, in steps of $50L_{\odot}$
 - (b) For high-mass range = $50L_{\odot}$ to $300L_{\odot}$, in steps of $50L_{\odot}$
- (iv) Effective temperature (T_{eff}) = 4000K to 8000K, in steps of 50K.

This results in a combination of 20412 models per convective parameter set. BL Her stars belong to the low-mass population with masses $\sim 0.5M_{\odot} - 0.6M_{\odot}$ (Bhardwaj 2020). However, we also explore the possibility of higher mass BL Her stars in this study. In his survey of non-linear convective T2C models, Smolec (2016) computed a grid using $0.6M_{\odot}$ and $0.8M_{\odot}$. The effective temperature range chosen in the present study is much broader than the actual width of the instability strip to accurately estimate the edges of the instability strip. MESA-RSP may be used to compute models where the structure of the stellar envelope determines the pulsations (Paxton et al. 2019), without taking into consideration the detailed structure of the core. We begin with a computation of linear properties of the models with the same method as described in Smolec (2016) and Paxton et al. (2019). To this end, equilibrium static models are constructed with $ZXMLT_{\text{eff}}$ as the input stellar parameters and their linear stability analysis is conducted, which yields linear periods of the radial pulsation modes and their growth rates. The latter may be used to delineate the boundaries of the instability strip. The static models also serve as input for non-linear model integration. Fig. 1 shows the HRD of the grid of computed BL Her models with the convection parameter set A, showing the edges of the instability strip and the lines of constant fundamental mode period (linear value) equal to 1 and 4 days. The other convective parameter sets (B, C and D) show similar HRDs. A future paper will investigate linear results in greater detail.

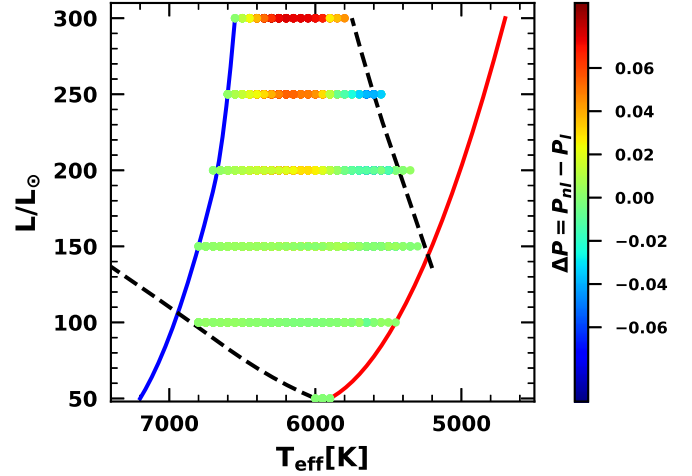


Figure 1. The Hertzsprung-Russell diagram of the grid of computed BL Her models with the convection parameter set A. The edges of the instability strip are estimated from the linear stability analysis and are shown with the blue and red solid lines. The dashed lines are lines of constant fundamental mode period (linear value) equal to 1 day (bottom) and 4 days (top). The dots represent the BL Her models used in this analysis while the colourbar shows the difference between the non-linear and linear period of the computed models, i.e., $\Delta P = P_{nl} - P_l$. The mean difference between the linear and non-linear periods in our models is ~ 0.02 days.

2.2 Non-Linear computations

We proceed with the non-linear computations for models that have positive growth rates of the radial fundamental mode and linear periods between 0.8 and 4.2 days. The period range is larger than considered for BL Her stars due to non-linear period changes. While non-linear period shifts expected for BL Her models are well below 0.05 days (see Fig. 6 in Smolec 2016), the changes of up to 0.2 days are noted for more luminous type II Cepheid models. Finally, we only select models with non-linear periods between 1 and 4 days as BL Her models, considering the typical period range of BL Her stars (Soszyński et al. 2018). We also confirm that non-linear period shifts are below 0.09 days in our models, with a mean non-linear period shift of ~ 0.02 days.

Note that the quantities that enter into energy and momentum equations of the MESA-RSP convection model depend on the free parameters described in Table 1; Paxton et al. (2019) found that the pulsation periods of the models weakly depend on the values of these free parameters. Therefore, a model with the same input parameters $ZXMLT_{\text{eff}}$ may have different non-linear periods across the different sets of convection parameters.

The non-linear model integration is carried for 4000 pulsation cycles; the control used for this terminating condition is RSP_max_num_periods in MESA-RSP. It is essential to check for full-amplitude stable pulsations of the models before obtaining the theoretical PL and PR relations. The model reaches full amplitude pulsation state when its kinetic energy per pulsation period remains constant. We can quantify that using the fractional growth of the kinetic energy per pulsation period Γ which should approach zero once stable pulsation state is reached. These pulsations may show some irregularities, e.g. period doubling effect or chaotic oscillations (Smolec et al. 2012; Smolec & Moskalik 2012, 2014). Since we are interested in stable single periodic oscillation, we also investigate whether the amplitude of radius variation ΔR and the pul-

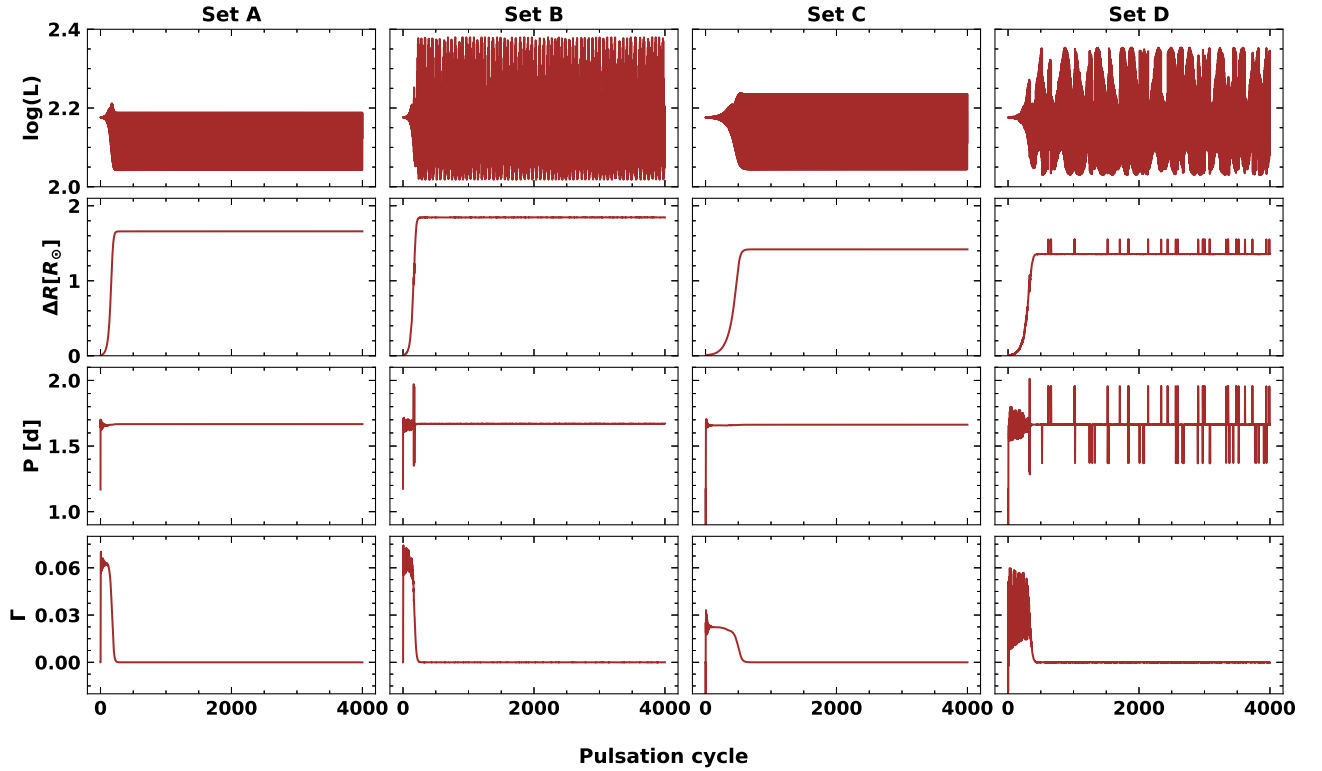


Figure 2. Luminosity $\log(L)$, amplitude of radius variation ΔR , period P and fractional growth rate Γ during 4000-cycle integrations of the BL Her model with input parameters, $Z = 0.013$, $X = 0.71847$, $M = 0.7M_{\odot}$, $L = 150L_{\odot}$, $T = 6350\text{K}$. The models with the same input parameters computed using sets A, B and C satisfy the condition of full-amplitude stable pulsation (ΔR , P and Γ do not vary by more than 0.01 over the last ~ 100 -cycles of the total 4000-cycle integrations) and are accepted for the analysis while the model computed using Set D is rejected.

sation period P computed on a cycle to cycle basis is stable. For our study, the condition of full-amplitude stable pulsation is satisfied and the model is accepted when its ΔR , P and Γ do not vary by more than 0.01 over the last ~ 100 -cycles of the total 4000-cycle integrations, failing which the model is rejected from further analysis. Fig. 2 shows an example for one particular model- while sets A, B and C exhibit full-amplitude stable pulsations and are accepted, the set D model is most likely chaotic and is rejected from our analysis. The number of models accepted in sets B and D is much less than in sets A and C. The sets B and D include radiative cooling with the parameter $\gamma_r = 2\sqrt{3}$, while this parameter is set to zero in the sets A and C. Table 3 summarises the number of BL Her models for each convection parameter set.

We note that the higher stellar mass ($>0.6M_{\odot}$) and lower metallicity ($Z=0.00014$) considered in our work is typical of Zero Age Horizontal Branch or evolved RR Lyrae stars. However, as discussed in Braga et al. (2020), the separation between RR Lyrae and T2Cs is a long-standing problem. A threshold of period ~ 1 day typically separates the two classes of pulsating variable stars (Soszyński et al. 2008, 2014). Braga et al. (2020) report the star V92 in ω -Cen (with a period of 1.3 days) to be a candidate RR Lyrae star because its core is likely in the helium-burning phase. Given the evidence, it is rather difficult to separate completely unambiguously the two different classes of pulsating variables based on their chemical composition. It might be possible to separate RR Lyrae and BL Her stars based on their evolutionary status, although this is not easily done for field stars. However, in this work, we use the conventional clas-

Table 3. A summary of the number of BL Her models in each convection parameter set finally used in the analysis.

Condition	Set A	Set B	Set C	Set D
Total $ZXMLT_{\text{eff}}$ combinations	20412	20412	20412	20412
(Models computed in the linear grid)				
Models with positive growth rate of the F-mode and with linear period: $0.8 \leq P \leq 4.2$	4481	4356	4061	4192
(Models computed in the non-linear grid)				
Models with non-linear period: $1 \leq P \leq 4$	4049	3854	3629	3678
Models with full-amplitude stable pulsation [†]	3266	2260	2632	2122

[†] Satisfies the condition that the amplitude of radius variation ΔR , period P and fractional growth rate Γ do not vary by more than 0.01 over the last ~ 100 -cycles of the total 4000-cycle integrations. For a clear, pictorial representation of full-amplitude stable pulsation, the reader may refer to Fig. 2.

sification for BL Her variables as population II stars with pulsation period between 1 and 4 days (Soszyński et al. 2018).

2.3 Processing the data

The details on the transformation of bolometric light curves into optical and NIR bands is given in Paxton et al. (2018) and is briefly summarised here. The luminosity $\log_{10}(L/L_{\odot})$ obtained from the non-linear computations of the models is converted to the absolute bolometric magnitude (M_{bol}) of the model using:

$$M_{\text{bol}} = M_{\text{bol},\odot} - 2.5 \log_{10}(L/L_{\odot}), \quad (1)$$

where $M_{\text{bol},\odot} = 4.74$ (Mamajek et al. 2015) is the absolute bolometric magnitude of the Sun. The absolute bolometric magnitude is then transformed into the absolute magnitude M_λ in a given band λ using:

$$M_\lambda = M_{\text{bol}} - BC_\lambda, \quad (2)$$

where BC_λ is the bolometric correction for band λ . MESA provides pre-computed bolometric correction tables where the bolometric correction is defined as a function of the stellar photosphere. For given stellar photosphere parameters, the bolometric correction table is interpolated over $\log(T)$, $\log(g)$ and the metallicity $[M/H]$ within the parameter range of that table. We use the pre-processed table from Lejeune et al. (1998) which provides bolometric corrections over the parameter range $2000 \leq T_{\text{eff}}(\text{K}) \leq 50,000$, $-1.02 \leq \log(g)(\text{cm s}^{-2}) \leq 5.0$, and $-5.0 \leq [M/H] \leq 1.0$ and for the Johnson-Cousins-Class bands $UBVR_cI_cJHKLL'M$. The minimal impact of adopted transformations on the mean-light properties at wavelengths longer than V -band is discussed in Appendix A.

The multi-wavelength theoretical light-curves of the accepted models are fitted with the Fourier sine series (see example, Deb & Singh 2009; Bhardwaj et al. 2015; Das et al. 2018) of the form:

$$m(x) = m_0 + \sum_{k=1}^N A_k \sin(2\pi kx + \phi_k), \quad (3)$$

where x is the pulsation phase, m_0 is the mean magnitude and N is the order of the fit ($N = 20$). Table 4 summarises the input stellar parameters of the BL Her models used in this analysis, along with the multi-wavelength absolute mean magnitudes obtained from the Fourier fitting. An example of light-curves for a BL Her model obtained using MESA-RSP over multiple wavelengths is presented in Fig. 3.

3 PERIOD-LUMINOSITY RELATIONS

The mean magnitudes obtained from Fourier fitting of the theoretical light-curves of the BL Her models are used to derive multi-wavelength PL relations of the mathematical form:

$$M_\lambda = a \log(P) + b, \quad (4)$$

where, M_λ refers to the absolute magnitude in a given band, λ .

3.1 Effect of convection parameters on PL relations

To study the effect of convection parameters on the PL relations, we use the standard t -test to check the statistical equivalence of the slopes from PL relations of the BL Her models obtained using different convective parameter sets. A detailed description of the test is provided in Ngeow et al. (2015) and Das et al. (2020) and is summarised here briefly. The T statistic to compare slopes, \hat{W} of two linear regressions with sample sizes, n and m , respectively is defined as:

$$T = \frac{\hat{W}_n - \hat{W}_m}{\sqrt{\text{Var}(\hat{W}_n) + \text{Var}(\hat{W}_m)}}, \quad (5)$$

where $\text{Var}(\hat{W})$ is the variance of the slope. We reject the null hypothesis of equivalent slopes if $T > t_{\alpha/2,\nu}$ or the probability of the observed value of the T statistic is $p < 0.05$. $t_{\alpha/2,\nu}$ is the critical value under the two-tailed t -distribution with 95% confidence limit ($\alpha=0.05$) and degrees of freedom, $\nu = n + m - 4$.

Table 5 lists the statistical comparison of the multi-wavelength

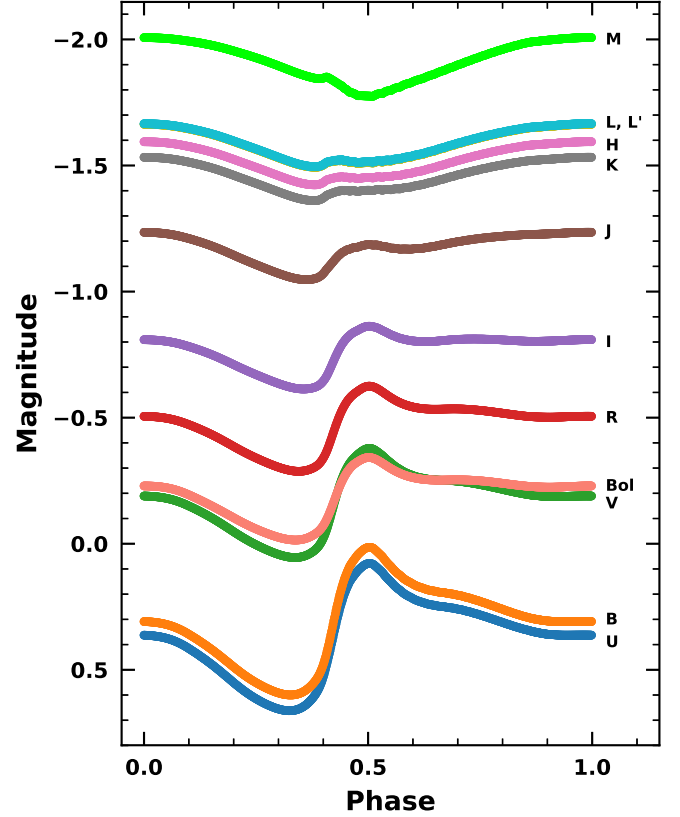


Figure 3. An example of the multi-wavelength light-curves for the BL Her model with input parameters, $Z = 0.00424$, $X = 0.74073$, $M = 0.80M_\odot$, $L = 100L_\odot$, $T = 6050\text{K}$ using convective parameter set A.

PL relation slopes of the BL Her models with respect to literature values. The BL Her models with radiative cooling (sets B and D) exhibit statistically similar PL slopes at any given wavelength, except in the U -band while those without radiative cooling (sets A and C) have statistically similar PL slopes only in the HLL' bands. BL Her models computed with different convection parameters do show differences in the slopes of the PL relations at a given wavelength. However, most empirical PL relations are consistent with theoretical PL relations based on any set of convection parameter. The PL slopes obtained for the BL Her stars in the Galactic bulge by Bhardwaj et al. (2017b) and in the SMC by Matsunaga et al. (2009) are statistically similar with those obtained from the BL Her models using all four sets of convection parameters and across JHK_S bands. Our models in all four convection parameter sets show statistically different PL slopes from the PL slope obtained by Matsunaga et al. (2006) for BL Her stars in the Globular clusters in the J -band; however, they exhibit statistically similar PL slopes in the HK_S bands. For the BL Her stars in the LMC, PL relations in the J -band show similar slopes between empirical data and models using all four sets of convection parameters; however, PL slopes of the models with sets B and D seem to match better with empirical relations in the HK_S bands. The bolometric PL relations obtained by Groenewegen & Jurkovic (2017b) for BL Her stars in the Magellanic Clouds show statistically similar slopes with models of different convection parameter sets, except for models computed with set A when the observed BL Her stars in the LMC and the SMC are

Table 4. A summary of the BL Her models used in this analysis computed using MESA-RSP. The columns provide the input parameters ($ZXMLT_{\text{eff}}$), the convection parameter set used, logarithmic pulsation period, logarithmic radius and the absolute mean magnitudes in the bands $UBVR_cI_cJHKLL'M$ and the bolometric.

Z	X	M/M _⊙	L/L _⊙	T _{eff} (K)	Convection Set	log(P)	log(R)	M _U	M _B	M _V	M _R	M _I	M _J	M _H	M _K	M _L	M _{L'}	M _M	M _{Bol}
0.00014	0.75115	0.50	50	5950	A	0.011	0.826	0.971	1.087	0.660	0.350	0.033	-0.412	-0.793	-0.732	-0.867	-0.870	-1.242	0.493
0.00014	0.75115	0.50	100	5650	A	0.367	1.024	0.382	0.452	-0.051	-0.411	-0.774	-1.259	-1.700	-1.627	-1.782	-1.787	-2.223	-0.257
...
0.00014	0.75115	0.50	100	5700	B	0.355	1.018	0.351	0.428	-0.060	-0.413	-0.770	-1.246	-1.677	-1.606	-1.757	-1.762	-2.187	-0.258
0.00014	0.75115	0.50	100	5750	B	0.336	1.013	0.342	0.417	-0.064	-0.411	-0.761	-1.230	-1.653	-1.583	-1.733	-1.737	-2.155	-0.256
...
0.00014	0.75115	0.50	50	5850	C	0.059	0.857	1.036	1.159	0.689	0.346	-0.003	-0.463	-0.879	-0.813	-0.957	-0.961	-1.370	0.493
0.00014	0.75115	0.50	50	5900	C	0.038	0.848	1.015	1.137	0.681	0.348	0.009	-0.446	-0.850	-0.786	-0.927	-0.931	-1.328	0.493
...
0.00014	0.75115	0.50	50	5900	D	0.039	0.848	1.012	1.135	0.680	0.347	0.008	-0.445	-0.849	-0.786	-0.926	-0.930	-1.325	0.493
0.00014	0.75115	0.50	50	5950	D	0.019	0.839	0.994	1.114	0.672	0.349	0.020	-0.430	-0.823	-0.761	-0.899	-0.902	-1.287	0.493
...

Note: This table is available entirely in a machine-readable form in the online journal as supporting information.

considered together. The fact that the PL slopes are statistically different between different sets of models, but empirically determined PL slopes are still compatible with all four sets of model PL slopes tells us that the models have lower uncertainty and scatter. Larger and more precise observational datasets are necessary to constrain the best fitting model parameters. From Table 5, we find that the PL slopes from the BL Her models become steeper with increasing wavelengths. This is similar to RR Lyrae as shown empirically in Beaton et al. (2018); Neeley et al. (2017); Bhardwaj et al. (2020). The dispersion in the theoretical PL relations for BL Hers decreases significantly on moving from optical to infrared wavelengths and becomes statistically similar for wavelengths longer than H -band. A similar decrease of intrinsic dispersion of the PL relations when changing from the optical to infrared bands has been reported by Neeley et al. (2017) based on RR Lyrae models from Marconi et al. (2015), and is also seen in empirical PL relations of RR Lyrae (e.g. Bhardwaj et al. 2020). This trend in dispersion is expected because of the stronger temperature sensitivity of the bolometric correction in the near-infrared, resulting in brighter magnitudes of BL Hers at cooler effective temperatures (Bono et al. 2003) and a marginal effect of the intrinsic temperature width of the instability strip on the infrared PL relations. In addition, the width of the instability strip itself decreases at longer wavelengths, resulting in smaller dispersion of PL relations (Catelan et al. 2004; Madore & Freedman 2012; Marconi et al. 2015). We also observe that the models computed using set B have the smallest dispersion in their PL relations in all the bands.

3.2 Effect of metallicity on PL relations

To quantify the effect of metallicity on the PL relations, we obtain PLZ relations for the BL Her models of the mathematical form:

$$M_\lambda = a + b \log(P) + c[\text{Fe}/\text{H}] \quad (6)$$

The results of the PLZ relations from the BL Her models for different wavelengths using different convective parameter sets is summarised in Table 6. The coefficients for the metallicity term from these relations suggest strong dependence of PL relations on metallicity in U and B bands but only modest effect at longer wavelengths. This result holds true for the four different convective parameter sets A, B, C and D. The weak or no dependence of PL relations on metallicity, especially at longer wavelengths is in agreement with earlier empirical evidence from Matsunaga et al. (2006) and Groenewegen & Jurkovic (2017b). Matsunaga et al. (2006) had studied the effect of metallicity on the PL relations of T2Cs in the GGCs in the NIR JHK_s bands while Groenewegen & Jurkovic

(2017b) had investigated the bolometric relations for T2Cs in the Magellanic Clouds. Table 6 also shows the theoretical PLZ relations obtained by Di Criscienzo et al. (2007) for BL Her models in the IJK bands. However, we note here that Di Criscienzo et al. (2007) use BL Her models with $-2.62 \text{ dex} \leq [\text{Fe}/\text{H}] \leq -0.66 \text{ dex}$ and $0.8 < P(\text{days}) < 8$ in their study.

The minimal dependence of metallicity on the PL relation in the V -band onward is very interesting. A possible reason for significant metallicity dependence in U and B -band could be that the effect of adopted model atmospheres on the transformations of bolometric light curves is significant at these wavelengths, as discussed in Appendix A. To further investigate the dependence on metallicity, we separated models in low-metallicity ($Z = 0.00014, 0.00043, 0.00061, 0.00135$) and high-metallicity ($Z = 0.00424, 0.00834, 0.01300$) regime. The results of PLZ relations for different convection sets are listed in Appendix Tables B1 and B2. For the convection set A, we find that in the low-metallicity regime, only the U -band PL relation displays a statistically significant dependence on metallicity. However, both U and B -band PL relations display a clear dependence on metallicity in the high-metallicity regime. The metallicity coefficient of V -band PL relation is consistent with zero even for high metallicities. However, the PL relations based on bolometric magnitudes show a marginal dependence on metallicity for convection set A which becomes consistent with zero for convection set D. This hints that the metallicity effects become significant in U and B -bands because of the increasing sensitivity of bolometric corrections to metallicities at wavelengths shorter than V -band (Gray 2005; Kudritzki et al. 2008). Furthermore, the zero-point of PL relations based on V -band and bolometric magnitudes are similar but the difference in slopes is significant at the 3σ level indicating a possible dependence on period. This could be because bolometric corrections depend not only on metallicities but also on gravity and temperature (or colour) (Kudritzki et al. 2008) where the latter may contribute to the dependence on the period through period-colour relations. We emphasize that the bolometric corrections of Lejeune et al. (1998) essentially come from the theoretical SEDs where the full coverage of the atmospheric parameters is ensured by combining the synthetic spectra from the Kurucz (1970) atmospheric models, supplemented with M giants spectra from Fluks et al. (1994) and Bessell et al. (1989, 1991) and spectra of M dwarfs from Allard & Hauschildt (1995) at low temperatures. However, a detailed investigation of the impact of different model atmospheres and the adopted bolometric corrections on the PL relations is beyond the scope of the present study.

Fig. 4 presents the PL relations of the BL Her models with different chemical compositions across different wavelengths for the

Table 5. Comparison of the slopes of the period-luminosity relations for BL Her stars of the mathematical form $M_I = a \log(P) + b$. N is the total number of stars and the number in parentheses indicates the number of outliers. $|T|$ represents the observed value of the t -statistic, and $p(t)$ gives the probability of acceptance of the null hypothesis (equal slopes). The bold-faced entries indicate that the null hypothesis of the equivalent PL slopes can be rejected.

Band	Source	a	b	σ	N	Reference [‡]	Theoretical/ Empirical	$(T , p(t))$ w.r.t.			
								Set A	Set B	Set C	Set D
U	Z _{all} (Set A)	-0.841±0.044	0.185±0.015	0.391	3266	TW	Theoretical
U	Z _{all} (Set B)	-0.596±0.046	0.215±0.015	0.353	2260	TW	Theoretical	(3.846,0.0)
U	Z _{all} (Set C)	-0.422±0.051	0.298±0.018	0.428	2632	TW	Theoretical	(6.219,0.0)	(2.512,0.006)
U	Z _{all} (Set D)	-0.369±0.053	0.309±0.018	0.409	2122	TW	Theoretical	(6.851,0.0)	(3.213,0.001)	(0.722,0.235)	...
B	Z _{all} (Set A)	-1.166±0.04	0.187±0.014	0.351	3266	TW	Theoretical
B	Z _{all} (Set B)	-0.896±0.041	0.209±0.013	0.311	2260	TW	Theoretical	(4.764,0.0)
B	Z _{all} (Set C)	-0.942±0.043	0.33±0.015	0.359	2632	TW	Theoretical	(3.843,0.0)	(0.791,0.214)
B	Z _{all} (Set D)	-0.805±0.044	0.324±0.015	0.339	2122	TW	Theoretical	(6.1,0.0)	(1.508,0.066)	(2.235,0.013)	...
V	Z _{all} (Set A)	-1.616±0.032	-0.14±0.011	0.284	3266	TW	Theoretical
V	Z _{all} (Set B)	-1.374±0.034	-0.134±0.011	0.256	2260	TW	Theoretical	(5.221,0.0)
V	Z _{all} (Set C)	-1.487±0.034	-0.031±0.012	0.288	2632	TW	Theoretical	(2.761,0.003)	(2.343,0.01)
V	Z _{all} (Set D)	-1.337±0.036	-0.043±0.012	0.275	2122	TW	Theoretical	(5.829,0.0)	(0.757,0.225)	(3.023,0.001)	...
R	Z _{all} (Set A)	-1.853±0.028	-0.364±0.01	0.248	3266	TW	Theoretical
R	Z _{all} (Set B)	-1.634±0.03	-0.365±0.01	0.227	2260	TW	Theoretical	(5.357,0.0)
R	Z _{all} (Set C)	-1.739±0.03	-0.281±0.01	0.254	2632	TW	Theoretical	(2.774,0.003)	(2.463,0.007)
R	Z _{all} (Set D)	-1.6±0.032	-0.293±0.011	0.243	2122	TW	Theoretical	(5.995,0.0)	(0.783,0.217)	(3.169,0.001)	...
I	Z _{all} (Set A)	-2.043±0.025	-0.592±0.008	0.219	3266	TW	Theoretical
I	Z _{all} (Set B)	-1.848±0.027	-0.599±0.009	0.203	2260	TW	Theoretical	(5.386,0.0)
I	Z _{all} (Set C)	-1.932±0.027	-0.534±0.009	0.226	2632	TW	Theoretical	(3.05,0.001)	(2.223,0.013)
I	Z _{all} (Set D)	-1.81±0.028	-0.545±0.01	0.218	2122	TW	Theoretical	(6.225,0.0)	(0.976,0.165)	(3.129,0.001)	...
J	Z _{all} (Set A)	-2.303±0.021	-0.914±0.007	0.186	3266	TW	Theoretical
J	Z _{all} (Set B)	-2.131±0.023	-0.928±0.008	0.177	2260	TW	Theoretical	(5.505,0.0)
J	Z _{all} (Set C)	-2.239±0.023	-0.877±0.008	0.19	2632	TW	Theoretical	(2.067,0.019)	(3.332,0.0)
J	Z _{all} (Set D)	-2.122±0.024	-0.89±0.008	0.187	2122	TW	Theoretical	(5.617,0.0)	(0.243,0.404)	(3.497,0.0)	...
J	Globular clusters	-2.959±0.313	-1.541±0.041 (@0.3)*	0.11	7	M06	Empirical	(2.091,0.018)	(2.638,0.004)	(2.294,0.011)	(2.666,0.004)
J	Galactic bulge	-2.387±0.164	11.393±0.132 (@1.0) [‡]	0.347	106	B17b	Empirical	(0.508,0.306)	(1.546,0.061)	(0.894,0.186)	(1.599,0.055)
J	LMC	-2.164±0.240	17.131±0.038 (@0.3)*	0.25	55	M09	Empirical	(0.577,0.282)	(0.137,0.446)	(0.311,0.378)	(0.174,0.431)
J	LMC	-2.294±0.153	15.375±0.113 (@1.0) [‡]	0.202	55	B17a	Empirical	(0.058,0.477)	(1.054,0.146)	(0.355,0.361)	(1.111,0.133)
J	SMC (IRSF only)	-2.545±0.764	17.393±0.112 (@0.3)*	0.41	15	M11	Empirical	(0.317,0.376)	(0.542,0.294)	(0.4,0.345)	(0.553,0.29)
J	SMC (IRSF+NTT)	-2.690±0.488	17.325±0.069 (@0.3)*	0.36	31	M11	Empirical	(0.792,0.214)	(1.144,0.126)	(0.923,0.178)	(1.163,0.122)
H	Z _{all} (Set A)	-2.57±0.018	-1.17±0.006	0.157	3266	TW	Theoretical
H	Z _{all} (Set B)	-2.429±0.02	-1.192±0.007	0.154	2260	TW	Theoretical	(5.236,0.0)
H	Z _{all} (Set C)	-2.529±0.019	-1.162±0.007	0.16	2632	TW	Theoretical	(1.568,0.058)	(3.587,0.0)
H	Z _{all} (Set D)	-2.432±0.021	-1.175±0.007	0.162	2122	TW	Theoretical	(5.048,0.0)	(0.081,0.468)	(3.439,0.0)	...
H	Globular clusters	-2.335±0.335	-1.847±0.044 (@0.3)*	0.12	7	M06	Empirical	(0.7,0.242)	(0.28,0.39)	(0.578,0.282)	(0.289,0.386)
H	Galactic bulge	-2.591±0.163	11.019±0.130 (@1.0) [‡]	0.353	104	B17b	Empirical	(0.128,0.449)	(0.986,0.162)	(0.378,0.353)	(0.967,0.167)
H	LMC	-2.259±0.248	16.857±0.039 (@0.3)*	0.26	54	M09	Empirical	(1.251,0.106)	(0.683,0.247)	(1.086,0.139)	(0.695,0.244)
H	LMC	-2.088±0.214	15.218±0.163 (@1.0) [‡]	0.296	52	B17a	Empirical	(2.244,0.012)	(1.587,0.056)	(2.053,0.02)	(1.6,0.055)
H	SMC (IRSF only)	-2.765±0.731	17.080±0.108 (@0.3)*	0.40	15	M11	Empirical	(0.267,0.395)	(0.459,0.323)	(0.323,0.373)	(0.455,0.325)
K	Z _{all} (Set A)	-2.528±0.018	-1.124±0.006	0.16	3266	TW	Theoretical
K	Z _{all} (Set B)	-2.383±0.021	-1.144±0.007	0.157	2260	TW	Theoretical	(5.308,0.0)
K	Z _{all} (Set C)	-2.483±0.02	-1.112±0.007	0.164	2632	TW	Theoretical	(1.7,0.045)	(3.526,0.0)
K	Z _{all} (Set D)	-2.383±0.021	-1.125±0.007	0.165	2122	TW	Theoretical	(5.194,0.0)	(0.008,0.497)	(3.453,0.0)	...
K _S	Globular clusters	-2.294±0.294	-1.864±0.039 (@0.3)*	0.10	7	M06	Empirical	(0.794,0.214)	(0.302,0.381)	(0.641,0.261)	(0.302,0.381)
K _S	Galactic bulge	-2.362±0.170	11.071±0.133 (@1.0) [‡]	0.294	108	B17b	Empirical	(0.971,0.166)	(0.123,0.451)	(0.707,0.24)	(0.123,0.451)
K _S	LMC	-1.992±0.278	16.733±0.040 (@0.3)*	0.26	47	M09	Empirical	(1.924,0.027)	(1.402,0.081)	(1.762,0.039)	(1.402,0.081)
K _S	LMC	-2.083±0.154	15.162±0.114 (@1.0) [‡]	0.262	47	B17a	Empirical	(2.87,0.002)	(0.93,0.027)	(2.76,0.005)	(1.93,0.027)
K _S	SMC (IRSF only)	-2.096±0.732	16.933±0.104 (@0.3)*	0.37	13	M11	Empirical	(0.59,0.278)	(0.392,0.348)	(0.528,0.299)	(0.392,0.348)
K _S	SMC (IRSF+NTT)	-2.553±0.444	16.924±0.061 (@0.3)*	0.32	29	M11	Empirical	(0.056,0.478)	(0.382,0.351)	(0.157,0.438)	(0.382,0.351)
L	Z _{all} (Set A)	-2.599±0.017	-1.231±0.006	0.155	3266	TW	Theoretical
L	Z _{all} (Set B)	-2.461±0.02	-1.253±0.007	0.153	2260	TW	Theoretical	(5.195,0.0)
L	Z _{all} (Set C)	-2.56±0.019	-1.226±0.007	0.158	2632	TW	Theoretical	(1.509,0.066)	(3.607,0.0)
L	Z _{all} (Set D)	-2.464±0.021	-1.238±0.007	0.16	2122	TW	Theoretical	(4.977,0.0)	(0.113,0.455)	(3.427,0.0)	...
L'	Z _{all} (Set A)	-2.599±0.017	-1.234±0.006	0.155	3266	TW	Theoretical
L'	Z _{all} (Set B)	-2.461±0.02	-1.256±0.007	0.153	2260	TW	Theoretical	(5.173,0.0)
L'	Z _{all} (Set C)	-2.561±0.019	-1.229±0.007	0.158	2632	TW	Theoretical	(1.477,0.07)	(3.617,0.0)
L'	Z _{all} (Set D)	-2.465±0.021	-1.241±0.007	0.16	2122	TW	Theoretical	(4.933,0.0)	(0.134,0.447)	(3.416,0.0)	...
M	Z _{all} (Set A)	-2.802±0.016	-1.492±0.006	0.144	3266	TW	Theoretical
M	Z _{all} (Set B)	-2.695±0.019	-1.519±0.006	0.145	2260	TW	Theoretical	(4.277,0.0)
M	Z _{all} (Set C)	-2.759±0.018	-1.514±0.006	0.148	2632	TW	Theoretical	(1.81,0.035)	(2.449,0.007)
M	Z _{all} (Set D)	-2.692±0.02	-1.523±0.007	0.151	2122	TW	Theoretical	(4.316,0.0)	(0.118,0.453)	(2.524,0.006)	...
Bolometric	Z _{all} (Set A)	-1.799±0.028	-0.181±0.01	0.253	3266	TW	Theoretical
Bolometric	Z _{all} (Set B)	-1.581±0.03	-0.18±0.01	0.231	2260	TW	Theoretical	(5.245,0.0)
Bolometric	Z _{all} (Set C)	-1.693±0.031	-0.094±0.011	0.256	2632	TW	Theoretical	(2.532,0.006)	(2.609,0.005)
Bolometric	Z _{all} (Set D)	-1.559±0.032	-0.103±0.011	0.246	2122	TW	Theoretical	(5.625,0.0)	(0.512,0.304)	(3.051,0.001)	...
Bolometric	LMC	-1.749±0.200	0.141±0.051	0.274	57(4)	G17	Empirical	(0.248,0.402)	(0.831,0.203)	(0.277,0.391)	(0.938,0.174)
Bolometric	SMC	-0.691±0.717	-0.250±0.176	0.302	15(2)	G17	Empirical	(1.544,0.061)	(1.24,0.108)	(1.396,0.081)	(1.209,0.113)
Bolometric	MCs	-1.326±0.257	-0.027±0.065	0.282	72(6)	G17	Empirical	(1.83,0.034)	(0.986,0.162)	(1.418,0.078)	(0.9,0.184)

[‡] TW=This work; M06=Matsunaga et al. (2006); M09=Matsunaga et al. (2009); M11=Matsunaga et al. (2011); B17a=Bhardwaj et al. (2017a); B17b=Bhardwaj et al. (2017b); G17=Groenewegen & Jurkovic (2017b)

* Zero point at $\log(P) = 0.3$

[†] Zero point at $\log(P) = 1.0$

Table 6. *PLZ* relations for BL Her models of the mathematical form $M_{\lambda} = a + b \log(P) + c[\text{Fe}/\text{H}]$ for different wavelengths using different convective parameter sets.

Band	a	b	c	σ	N
Convection set A					
U	0.438 ± 0.017	-0.998 ± 0.041	0.234 ± 0.009	0.357	3266
B	0.276 ± 0.016	-1.221 ± 0.04	0.082 ± 0.009	0.347	3266
V	-0.134 ± 0.013	-1.62 ± 0.032	0.006 ± 0.007	0.284	3266
R	-0.372 ± 0.012	-1.848 ± 0.028	-0.007 ± 0.006	0.248	3266
I	-0.593 ± 0.01	-2.043 ± 0.025	-0.001 ± 0.006	0.219	3266
J	-0.908 ± 0.009	-2.306 ± 0.021	0.005 ± 0.005	0.186	3266
H	-1.154 ± 0.007	-2.58 ± 0.018	0.015 ± 0.004	0.156	3266
K	-1.107 ± 0.008	-2.539 ± 0.018	0.015 ± 0.004	0.16	3266
L	-1.212 ± 0.007	-2.611 ± 0.018	0.017 ± 0.004	0.154	3266
L'	-1.214 ± 0.007	-2.611 ± 0.018	0.019 ± 0.004	0.155	3266
M	-1.441 ± 0.007	-2.833 ± 0.016	0.047 ± 0.004	0.14	3266
Bolometric	-0.131 ± 0.012	-1.83 ± 0.029	0.047 ± 0.006	0.251	3266
Convection set B					
U	0.454 ± 0.017	-0.706 ± 0.042	0.234 ± 0.01	0.315	2260
B	0.284 ± 0.016	-0.93 ± 0.04	0.073 ± 0.009	0.307	2260
V	-0.138 ± 0.014	-1.372 ± 0.034	-0.004 ± 0.008	0.256	2260
R	-0.381 ± 0.012	-1.627 ± 0.03	-0.016 ± 0.007	0.227	2260
I	-0.607 ± 0.011	-1.844 ± 0.027	-0.008 ± 0.006	0.203	2260
J	-0.931 ± 0.009	-2.129 ± 0.023	-0.003 ± 0.005	0.177	2260
H	-1.184 ± 0.008	-2.433 ± 0.02	0.008 ± 0.005	0.154	2260
K	-1.136 ± 0.008	-2.387 ± 0.021	0.008 ± 0.005	0.157	2260
L	-1.242 ± 0.008	-2.466 ± 0.02	0.011 ± 0.005	0.153	2260
L'	-1.244 ± 0.008	-2.467 ± 0.02	0.012 ± 0.005	0.153	2260
M	-1.475 ± 0.008	-2.715 ± 0.019	0.043 ± 0.004	0.142	2260
Bolometric	-0.141 ± 0.012	-1.599 ± 0.03	0.037 ± 0.007	0.229	2260
Convection set C					
U	0.589 ± 0.02	-0.646 ± 0.047	0.271 ± 0.011	0.387	2632
B	0.423 ± 0.018	-1.014 ± 0.043	0.087 ± 0.01	0.354	2632
V	-0.029 ± 0.015	-1.488 ± 0.035	0.002 ± 0.008	0.288	2632
R	-0.294 ± 0.013	-1.729 ± 0.031	-0.012 ± 0.007	0.253	2632
I	-0.537 ± 0.012	-1.929 ± 0.027	-0.003 ± 0.007	0.226	2632
J	-0.878 ± 0.01	-2.238 ± 0.023	-0.001 ± 0.006	0.19	2632
H	-1.15 ± 0.008	-2.539 ± 0.019	0.011 ± 0.005	0.16	2632
K	-1.1 ± 0.008	-2.492 ± 0.02	0.011 ± 0.005	0.164	2632
L	-1.21 ± 0.008	-2.572 ± 0.019	0.015 ± 0.005	0.158	2632
L'	-1.211 ± 0.008	-2.574 ± 0.019	0.016 ± 0.005	0.158	2632
M	-1.456 ± 0.007	-2.803 ± 0.017	0.054 ± 0.004	0.143	2632
Bolometric	-0.047 ± 0.013	-1.729 ± 0.031	0.043 ± 0.007	0.254	2632
Convection set D					
U	0.588 ± 0.02	-0.527 ± 0.048	0.273 ± 0.012	0.364	2122
B	0.411 ± 0.018	-0.855 ± 0.044	0.086 ± 0.011	0.334	2122
V	-0.043 ± 0.015	-1.337 ± 0.036	-0.0 ± 0.009	0.275	2122
R	-0.307 ± 0.013	-1.593 ± 0.032	-0.013 ± 0.008	0.243	2122
I	-0.549 ± 0.012	-1.808 ± 0.029	-0.004 ± 0.007	0.218	2122
J	-0.892 ± 0.01	-2.122 ± 0.025	-0.002 ± 0.006	0.187	2122
H	-1.164 ± 0.009	-2.438 ± 0.021	0.011 ± 0.005	0.161	2122
K	-1.114 ± 0.009	-2.389 ± 0.022	0.01 ± 0.005	0.165	2122
L	-1.224 ± 0.009	-2.472 ± 0.021	0.014 ± 0.005	0.16	2122
L'	-1.225 ± 0.009	-2.474 ± 0.021	0.016 ± 0.005	0.16	2122
M	-1.468 ± 0.008	-2.723 ± 0.019	0.054 ± 0.005	0.147	2122
Bolometric	-0.062 ± 0.013	-1.582 ± 0.032	0.04 ± 0.008	0.244	2122
Theoretical relations from Di Criscienzo et al. (2007) [†]					
I	-0.26±0.19	-2.10±0.06	0.04±0.01	-	-
J	-0.64±0.13	-2.29±0.04	0.04±0.01	-	-
H	-0.95±0.06	-2.34±0.02	0.06±0.01	-	-
K	-0.97±0.06	-2.38±0.02	0.06±0.01	-	-

[†] For BL Her models with $-2.62 \text{ dex} \leq [\text{Fe}/\text{H}] \leq -0.66 \text{ dex}$ and $0.8 < P(\text{days}) < 8$

convective parameter set A. The other convection parameter sets (B, C and D) show similar *PL* relations as a function of metallicity and wavelength. From Fig. 4, we find that the different chemical compositions lead to statistically similar slopes of *PL* relations.

3.3 Period-Wesenheit relations

Wesenheit indices (Madore 1982) may be used as pseudo-magnitudes but with the added advantage that they are minimally affected by the uncertainties related to reddening corrections. A few empirical studies provide *PW* relations instead of *PL* relations (see example, Bhardwaj et al. 2017a). To facilitate the ease of comparison with empirical results, we provide theoretical *PW* relations for our models. For the magnitudes (m_{λ_1} and m_{λ_2}) in two bands (λ_1 and λ_2), the Wesenheit index may be defined as (Inno et al. 2013; Bhardwaj et al. 2016):

$$W(\lambda_2, \lambda_1) = m_{\lambda_1} - \left[\frac{A(\lambda_1)}{E(m_{\lambda_2} - m_{\lambda_1})} \right] \times (m_{\lambda_2} - m_{\lambda_1}), \quad (7)$$

where $\lambda_1 > \lambda_2$ and $A(\lambda_1)/E(m_{\lambda_2} - m_{\lambda_1})$ is the total-to-selective extinction for the given filters using a particular reddening law. We adopt the reddening law from Cardelli et al. (1989) and assume $R_V = A(V)/(A(B) - A(V)) = 3.23$. For our study, we combine five optical-NIR (*VIJHK*) mean magnitudes to obtain 10 Wesenheit indices using the selective absorption ratios (Inno et al. 2013): $A_I/A_V = 0.61$, $A_J/A_V = 0.29$, $A_H/A_V = 0.18$ and $A_K/A_V = 0.12$. We derive the corresponding *PW* relations of the mathematical form $W = a \log(P) + b$ for the BL Her models. The statistical comparison of the slopes from the theoretical NIR and optical-NIR *PW* relations of the BL Her models using different convection parameter sets and those from previous literature is provided in Table 7. Similar to the *PL* slopes, the BL Her models with radiative cooling (sets B and D) exhibit statistically similar *PW* slopes across all 10 Wesenheit indices, while the models without radiative cooling (sets A and C) present larger differences for W_{VI} and W_{HK} indices. The theoretical *PW* relations from the models are consistent with the empirical relations for BL Her stars in the LMC and the SMC (Matsunaga et al. 2009, 2011; Groenewegen & Jurkovic 2017b). We note here that the differences between the theoretical *PW* relations from the models are smaller than empirical uncertainties from the data.

4 PERIOD-RADIUS RELATIONS

The mean radius obtained from averaging the radius of the BL Her model over a pulsation cycle may be used for deriving theoretical *PR* relations for BL Her models of the mathematical form (Burki & Meylan 1986; Marconi & Di Criscienzo 2007):

$$\log(R/R_{\odot}) = \alpha \log(P) + \beta \quad (8)$$

4.1 Effect of convection parameters on *PR* relations

The *PR* relations for BL Her models for different chemical compositions using different convective parameter sets are summarised in Table 8. The slopes and intercepts of the *PR* relations obtained using different chemical compositions are found to be similar.

We use the statistical *t*-test (Eq. 5) to compare the slopes from the theoretical *PR* relations across different convection parameter sets with those obtained from previous studies. The results from this test are presented in Table 9. Models with sets A and C have statistically similar *PR* slopes while those with sets B and D show similar *PR* slopes. We also find the slopes from the theoretical *PR* relations of the BL Her models to be similar with those from the empirical results for the LMC and the SMC from Groenewegen & Jurkovic (2017b). Fig. 5 presents a comparison of the slopes and intercepts of the *PR* relations for the BL Her stars obtained from this work using

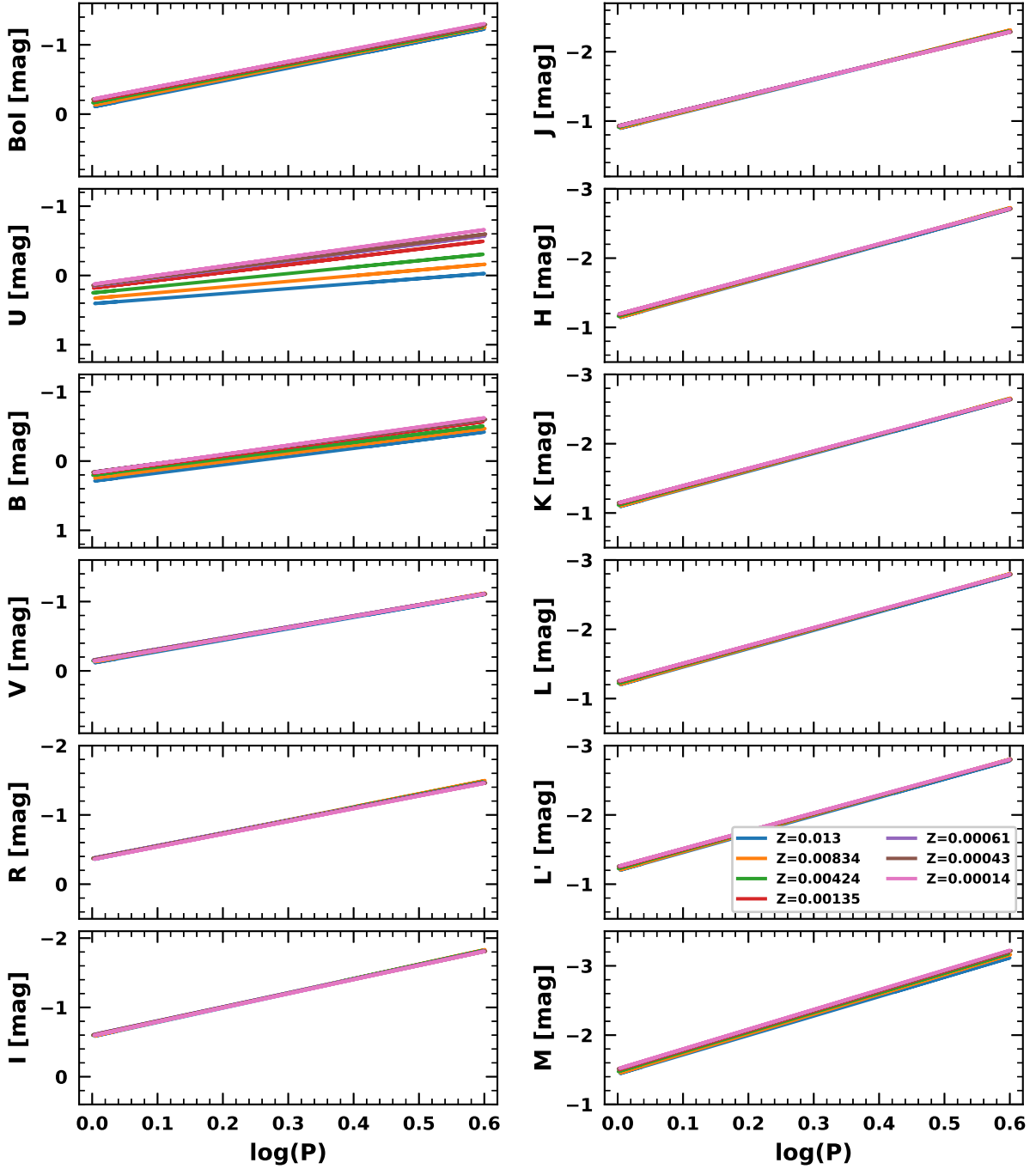


Figure 4. *PL* relations of the BL Her models with different chemical compositions across different wavelengths for the convective parameter set A. The y-scale is same (2.5 mag) in each panel for a relative comparison. The other convection parameter sets (B, C and D) show similar *PL* relations as a function of metallicity and wavelength.

four different convective parameter sets with those obtained from previous literature. We also use a subset of our BL Her models with the same input parameter space as that of Marconi & Di Criscienzo (2007) to compare the theoretical *PR* relations; the results are displayed in Fig.5.

4.2 Effect of metallicity on *PR* relations

To test for the effect of metallicity on the *PR* relations, we derive *PRZ* relations of the form:

$$\log(R/R_{\odot}) = \alpha + \beta \log(P) + \gamma[\text{Fe}/\text{H}] \quad (9)$$

Table 7. Comparison of the slopes of the NIR and optical-NIR PW relations for BL Her stars of the mathematical form $W = a \log(P) + b$. N is the total number of stars and the number in parentheses indicates the number of outliers. $|T|$ represents the observed value of the t -statistic, and $p(t)$ gives the probability of acceptance of the null hypothesis (equal slopes). The bold-faced entries indicate that the null hypothesis of the equivalent PL slopes can be rejected.

Band	Source	a	b	σ	N	Reference [‡]	Theoretical/ Empirical	(T , p(t)) w.r.t.			
								Set A	Set B	Set C	Set D
W _{VI}	Z _{all} (Set A)	-2.705±0.017	-1.292±0.006	0.147	3266	TW	Theoretical
W _{VI}	Z _{all} (Set B)	-2.582±0.019	-1.32±0.006	0.147	2260	TW	Theoretical	(4.877,0.0)
W _{VI}	Z _{all} (Set C)	-2.622±0.018	-1.314±0.006	0.153	2632	TW	Theoretical	(3.376,0.0)	(1.528,0.063)
W _{VI}	Z _{all} (Set D)	-2.542±0.02	-1.325±0.007	0.155	2122	TW	Theoretical	(6.273,0.0)	(1.417,0.078)	(2.945,0.002)	...
W _{VI}	LMC	-2.598±0.094	16.597±0.017 (@0.3) [†]	0.10	55	M09	Empirical	(1.125,0.13)	(0.169,0.433)	(0.253,0.4)	(0.579,0.281)
W _{VI}	LMC	-2.576±0.080	17.359±0.022	0.089	55(6)	G17	Empirical	(1.584,0.057)	(0.07,0.472)	(0.564,0.286)	(0.408,0.342)
W _{VI}	@LMC [†]	-2.669±0.137	17.347±0.038	0.170	74(4)	G17	Empirical	(0.263,0.396)	(0.631,0.264)	(0.338,0.368)	(0.915,0.18)
W _{VI}	SMC	-2.421±0.479	16.832±0.069 (@0.3) [†]	0.26	17	M11	Empirical	(0.593,0.277)	(0.335,0.369)	(0.42,0.337)	(0.253,0.4)
W _{VI}	SMC	-2.429±0.480	17.558±0.134	0.241	17(0)	G17	Empirical	(0.575,0.283)	(0.318,0.375)	(0.402,0.344)	(0.236,0.407)
W _{VJ}	Z _{all} (Set A)	-2.584±0.018	-1.23±0.006	0.156	3266	TW	Theoretical
W _{VJ}	Z _{all} (Set B)	-2.441±0.02	-1.254±0.007	0.154	2260	TW	Theoretical	(5.349,0.0)
W _{VJ}	Z _{all} (Set C)	-2.547±0.019	-1.224±0.007	0.16	2632	TW	Theoretical	(1.422,0.078)	(3.831,0.0)
W _{VJ}	Z _{all} (Set D)	-2.444±0.021	-1.238±0.007	0.161	2122	TW	Theoretical	(5.11,0.0)	(0.127,0.449)	(3.631,0.0)	...
W _{VH}	Z _{all} (Set A)	-2.78±0.016	-1.396±0.005	0.142	3266	TW	Theoretical
W _{VH}	Z _{all} (Set B)	-2.662±0.019	-1.424±0.006	0.143	2260	TW	Theoretical	(4.801,0.0)
W _{VH}	Z _{all} (Set C)	-2.759±0.017	-1.411±0.006	0.144	2632	TW	Theoretical	(0.907,0.182)	(3.82,0.0)
W _{VH}	Z _{all} (Set D)	-2.673±0.019	-1.424±0.007	0.148	2122	TW	Theoretical	(4.296,0.0)	(0.411,0.341)	(3.343,0.0)	...
W _{VK}	Z _{all} (Set A)	-2.647±0.017	-1.251±0.006	0.15	3266	TW	Theoretical
W _{VK}	Z _{all} (Set B)	-2.514±0.02	-1.276±0.006	0.15	2260	TW	Theoretical	(5.132,0.0)
W _{VK}	Z _{all} (Set C)	-2.613±0.018	-1.253±0.006	0.153	2632	TW	Theoretical	(1.378,0.084)	(3.68,0.0)
W _{VK}	Z _{all} (Set D)	-2.519±0.02	-1.266±0.007	0.156	2122	TW	Theoretical	(4.854,0.0)	(0.181,0.428)	(3.436,0.0)	...
W _{IJ}	Z _{all} (Set A)	-2.541±0.018	-1.209±0.006	0.161	3266	TW	Theoretical
W _{IJ}	Z _{all} (Set B)	-2.391±0.021	-1.231±0.007	0.158	2260	TW	Theoretical	(5.471,0.0)
W _{IJ}	Z _{all} (Set C)	-2.521±0.019	-1.193±0.007	0.163	2632	TW	Theoretical	(0.758,0.224)	(4.587,0.0)
W _{IJ}	Z _{all} (Set D)	-2.41±0.021	-1.208±0.007	0.165	2122	TW	Theoretical	(4.685,0.0)	(0.648,0.259)	(3.843,0.0)	...
W _{IH}	Z _{all} (Set A)	-2.792±0.016	-1.412±0.005	0.142	3266	TW	Theoretical
W _{IH}	Z _{all} (Set B)	-2.674±0.019	-1.44±0.006	0.143	2260	TW	Theoretical	(4.779,0.0)
W _{IH}	Z _{all} (Set C)	-2.78±0.017	-1.426±0.006	0.143	2632	TW	Theoretical	(0.479,0.316)	(4.203,0.0)
W _{IH}	Z _{all} (Set D)	-2.693±0.019	-1.439±0.007	0.147	2122	TW	Theoretical	(3.949,0.0)	(0.721,0.235)	(3.404,0.0)	...
W _{IK}	Z _{all} (Set A)	-2.645±0.017	-1.251±0.006	0.151	3266	TW	Theoretical
W _{IK}	Z _{all} (Set B)	-2.511±0.02	-1.275±0.006	0.15	2260	TW	Theoretical	(5.143,0.0)
W _{IK}	Z _{all} (Set C)	-2.615±0.018	-1.251±0.006	0.153	2632	TW	Theoretical	(1.18,0.119)	(3.88,0.0)
W _{IK}	Z _{all} (Set D)	-2.521±0.02	-1.264±0.007	0.156	2122	TW	Theoretical	(4.706,0.0)	(0.334,0.369)	(3.477,0.0)	...
W _{JH}	Z _{all} (Set A)	-3.006±0.015	-1.587±0.005	0.137	3266	TW	Theoretical
W _{JH}	Z _{all} (Set B)	-2.917±0.018	-1.621±0.006	0.139	2260	TW	Theoretical	(3.762,0.0)
W _{JH}	Z _{all} (Set C)	-3.003±0.016	-1.627±0.006	0.136	2632	TW	Theoretical	(0.146,0.442)	(3.544,0.0)
W _{JH}	Z _{all} (Set D)	-2.936±0.018	-1.639±0.006	0.142	2122	TW	Theoretical	(2.919,0.002)	(0.753,0.226)	(2.722,0.003)	...
W _{JK}	Z _{all} (Set A)	-2.684±0.017	-1.268±0.006	0.148	3266	TW	Theoretical
W _{JK}	Z _{all} (Set B)	-2.557±0.019	-1.294±0.006	0.147	2260	TW	Theoretical	(4.991,0.0)
W _{JK}	Z _{all} (Set C)	-2.652±0.018	-1.275±0.006	0.15	2632	TW	Theoretical	(1.329,0.092)	(3.597,0.0)
W _{JK}	Z _{all} (Set D)	-2.563±0.02	-1.287±0.007	0.153	2122	TW	Theoretical	(4.682,0.0)	(0.218,0.414)	(3.32,0.0)	...
W _{HK}	Z _{all} (Set A)	-2.448±0.019	-1.035±0.006	0.168	3266	TW	Theoretical
W _{HK}	Z _{all} (Set B)	-2.293±0.021	-1.054±0.007	0.163	2260	TW	Theoretical	(5.421,0.0)
W _{HK}	Z _{all} (Set C)	-2.394±0.02	-1.016±0.007	0.172	2632	TW	Theoretical	(1.932,0.027)	(3.407,0.0)
W _{HK}	Z _{all} (Set D)	-2.289±0.022	-1.029±0.008	0.171	2122	TW	Theoretical	(5.441,0.0)	(0.124,0.451)	(3.468,0.0)	...

[‡] TW=This work; M09=Matsunaga et al. (2009); M11=Matsunaga et al. (2011); G17=Groenewegen & Jurkovic (2017b)

* Zero point at $\log(P) = 0.3$

[†] The stars in the LMC plus the stars in the SMC placed at the distance of the LMC by a shift of 0.432 mag

for the four different convection parameter sets. We find the following relations for set A:

$$\log(R/R_{\odot}) = (0.879 \pm 0.001) + (0.581 \pm 0.003) \log(P) - (0.006 \pm 0.001)[\text{Fe}/\text{H}] \quad (N = 3266; \sigma = 0.029), \quad (10)$$

for set B:

$$\log(R/R_{\odot}) = (0.888 \pm 0.002) + (0.548 \pm 0.004) \log(P) - (0.006 \pm 0.001)[\text{Fe}/\text{H}] \quad (N = 2260; \sigma = 0.029), \quad (11)$$

for set C:

$$\log(R/R_{\odot}) = (0.881 \pm 0.001) + (0.579 \pm 0.003) \log(P) - (0.006 \pm 0.001)[\text{Fe}/\text{H}] \quad (N = 2632; \sigma = 0.028), \quad (12)$$

and for set D:

$$\log(R/R_{\odot}) = (0.886 \pm 0.002) + (0.554 \pm 0.004) \log(P) - (0.006 \pm 0.001)[\text{Fe}/\text{H}] \quad (N = 2122; \sigma = 0.029) \quad (13)$$

From Eqs. 10-13, we find the coefficients of the metallicity term to be very small for all four convection parameter sets and thus, we may conclude that there is weak dependence of PR relations on metallicity. This is in agreement with previous empirical results from Burki & Meylan (1986), Balog et al. (1997) and Groenewegen & Jurkovic (2017b). We also find that the dependency of PR relations on metallicity is identical for all four sets of convection parameters.

5 COMPARISON WITH RR LYRAE MODELS

RR Lyrae and BL Her stars are pulsating variables that belong to old stellar populations of similar chemical compositions. Both classes are population II pulsating stars and offer an important alternative

Table 8. Period-radius relations for BL Her models of the mathematical form $\log(R/R_{\odot}) = \alpha \log(P) + \beta$ for different chemical compositions using different convective parameter sets.

Source	α	β	σ	N
Convection set A				
Z=0.00014	0.574±0.009	0.892±0.003	0.029	434
Z=0.00043	0.572±0.009	0.891±0.003	0.029	432
Z=0.00061	0.574±0.009	0.89±0.003	0.029	431
Z=0.00135	0.576±0.009	0.887±0.003	0.029	437
Z=0.00424	0.584±0.009	0.882±0.003	0.029	466
Z=0.00834	0.594±0.008	0.876±0.003	0.028	515
Z=0.01300	0.588±0.007	0.875±0.003	0.027	551
Convection set B				
Z=0.00014	0.534±0.011	0.902±0.003	0.03	302
Z=0.00043	0.536±0.011	0.9±0.003	0.029	299
Z=0.00061	0.535±0.01	0.9±0.003	0.029	302
Z=0.00135	0.535±0.01	0.896±0.003	0.029	314
Z=0.00424	0.545±0.01	0.891±0.003	0.028	319
Z=0.00834	0.57±0.01	0.882±0.003	0.029	340
Z=0.01300	0.572±0.009	0.88±0.003	0.029	384
Convection set C				
Z=0.00014	0.56±0.011	0.897±0.003	0.029	314
Z=0.00043	0.563±0.011	0.895±0.003	0.029	321
Z=0.00061	0.565±0.01	0.894±0.003	0.029	324
Z=0.00135	0.572±0.01	0.891±0.003	0.028	333
Z=0.00424	0.576±0.009	0.885±0.003	0.028	380
Z=0.00834	0.598±0.008	0.876±0.003	0.027	444
Z=0.01300	0.599±0.008	0.872±0.003	0.028	516
Convection set D				
Z=0.00014	0.53±0.011	0.902±0.003	0.03	262
Z=0.00043	0.534±0.011	0.901±0.004	0.031	275
Z=0.00061	0.541±0.01	0.898±0.003	0.029	280
Z=0.00135	0.543±0.01	0.894±0.003	0.029	277
Z=0.00424	0.559±0.01	0.886±0.003	0.028	289
Z=0.00834	0.57±0.01	0.882±0.004	0.029	336
Z=0.01300	0.59±0.009	0.874±0.003	0.028	403

tool to classical Cepheids to calibrate the cosmic distance scale and evaluate the Hubble constant. [Majaess \(2010\)](#) presented preliminary evidence of a common PL relation for RR Lyrae and T2Cs. [Bhardwaj et al. \(2017a\)](#) showed that the PL relation of T2Cs in K -band when extended to periods less than 1 day follow the same PL relation as RR Lyrae stars. They also demonstrated that distances to the GGCs based on T2Cs are consistent with those based on horizontal branch (HB) stars. In the most recent study, [Braga et al. \(2020\)](#) derived PL relations of RR Lyrae and T2Cs in ω Cen and found empirical evidence that RRab and T2Cs indeed obey the same JHK_S PL relations.

To test this equivalence between RR Lyrae and T2Cs, we compare the theoretical relations from our BL Her models with the most recent grid of RR Lyrae models from [Marconi et al. \(2015\)](#). Table 10 presents the comparison of the PL slopes in $RIJK_S$ bands for RR Lyrae models from [Marconi et al. \(2015\)](#) with those obtained from the BL Her models of our work. The RR Lyrae models exhibit statistically similar PL slopes in the bands, $RIJK_S$ with those from the BL Her models computed using sets A and C. A possible explanation for the slopes not being statistically similar with BL Her models computed using sets B and D is that the RR Lyrae models from [Marconi et al. \(2015\)](#) are computed without radiative cooling. Our grid of BL Her models therefore supports the claim by [Braga et al. \(2020\)](#) that the equivalence of the PL relations of RR Lyrae and T2Cs gives us the opportunity of adopting RRLs+T2Cs together

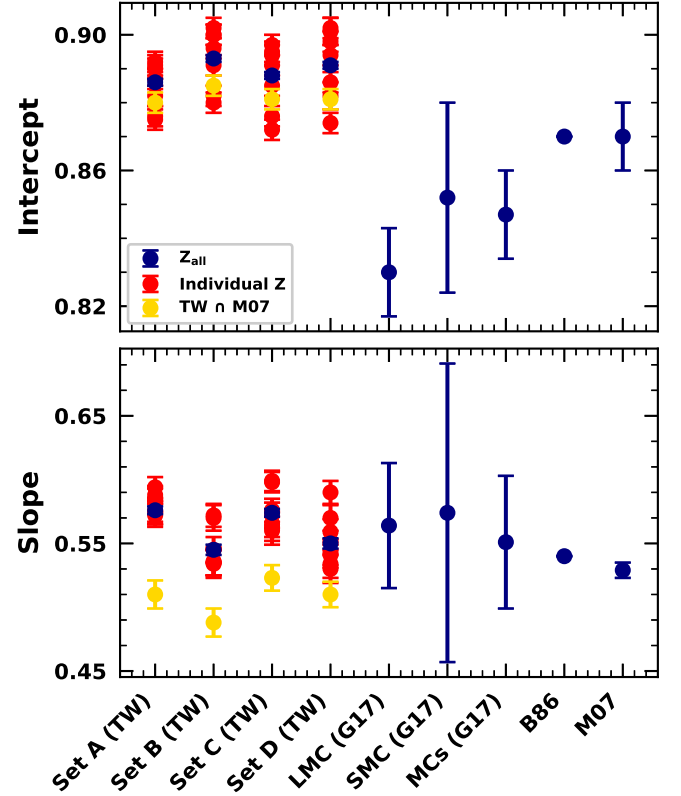


Figure 5. A comparison of the slopes and intercepts of the PR relations for the BL Her stars obtained from this work (TW) using four different convective parameter sets with those obtained from previous literature. The red dots refer to the slopes and intercepts of the PR relations obtained for the different chemical compositions individually, while the blue dots refer to the results obtained from considering the entire range of chemical compositions ($Z = 0.00014 - Z = 0.013$) together. The yellow dots represent the subset of the model grid of this work with the same parameter space as that of [Marconi & Di Criscienzo \(2007\)](#). G17, B86 and M07 refer to [Groenewegen & Jurkovic \(2017b\)](#), [Burki & Meylan \(1986\)](#) and [Marconi & Di Criscienzo \(2007\)](#), respectively.

as an alternative to classical Cepheids for the extragalactic distance scale calibration.

From Table 10, we also find that the PR slope of the RR Lyrae models from [Marconi et al. \(2015\)](#) is statistically similar with those obtained from the BL Her models in all four sets of convection parameters. This is in support of the result obtained by [Marconi et al. \(2015\)](#) where they found similar PR slopes for RR Lyrae models with theoretical and empirical BL Her PR slopes from [Marconi & Di Criscienzo \(2007\)](#) and [Burki & Meylan \(1986\)](#), respectively. This therefore suggests tight correlation of evolutionary and pulsational properties of the two classes of evolved low-mass radial variables. A detailed comparison of RR Lyrae and BL Her pulsation properties could be useful to probe an evolutionary scenario where BL Hers are HB stars that have evolved off the HB and are moving up the Asymptotic Giant Branch (AGB). BL Her stars may then be considered as the evolved component of RR Lyrae stars

Table 9. Comparison of the slopes of the PR relations for BL Her stars of the mathematical form $\log(R/R_{\odot}) = \alpha \log(P) + \beta$. N is the total number of stars and the number in parentheses indicates the number of outliers. $|T|$ represents the observed value of the t -statistic, and $p(t)$ gives the probability of acceptance of the null hypothesis (equal slopes). The bold-faced entries indicate that the null hypothesis of the equivalent PR slopes can be rejected.

Source	α	β	σ	N	Reference [‡]	Theoretical/ Empirical	$(T , p(t))$ w.r.t.			
							Set A	Set B	Set C	Set D
Z_{all} (Set A)	0.576±0.003	0.886±0.001	0.029	3266	TW	Theoretical
Z_{all} (Set B)	0.545±0.004	0.893±0.001	0.029	2260	TW	Theoretical	(6.278,0.0)
Z_{all} (Set C)	0.574±0.003	0.888±0.001	0.029	2632	TW	Theoretical	(0.588,0.278)	(5.595,0.0)
Z_{all} (Set D)	0.55±0.004	0.891±0.001	0.029	2122	TW	Theoretical	(5.17,0.0)	(1.046,0.148)	(4.509,0.0)	...
LMC	0.564±0.049	0.830±0.013	0.047	57(4)	G17	Empirical	(0.253,0.4)	(0.39,0.348)	(0.197,0.422)	(0.275,0.392)
SMC	0.574±0.117	0.852±0.028	0.056	17(0)	G17	Empirical	(0.021,0.492)	(0.249,0.402)	(0.003,0.499)	(0.201,0.42)
MCs	0.551±0.052	0.847±0.013	0.058	76(2)	G17	Empirical	(0.488,0.313)	(0.119,0.453)	(0.435,0.332)	(0.01,0.496)
Galactic T2Cs	0.54	0.87	-	-	B86*	Empirical	-	-	-	-
Z_{all}	0.529±0.006	0.87±0.01	-	-	M07*	Theoretical	-	-	-	-

[‡] TW=This work; G17=Groenewegen & Jurkovic (2017b); B86=Burki & Meylan (1986); M07=Marconi & Di Criscienzo (2007)

* Data insufficient to determine the value of the t -statistic and the associated probability value.

Marconi et al. (2011, 2015)². Marconi et al. (2015) cautions that this similarity between BL Her and RR Lyrae may not be extended over the entire metallicity range. We note here that Marconi et al. (2015) uses the convection formulation outlined in Stellingwerf (1982a,b) while MESA-RSP uses Kuhfuss (1986) turbulent convection theory; it is therefore interesting to obtain similar PL and PR results for RR Lyrae and BL Her models using different theories of convection.

6 SUMMARY AND CONCLUSION

We computed a very fine grid of BL Her models using the most recent, state-of-the-art stellar pulsation code, the MESA-RSP (Paxton et al. 2019). The grid encompasses a wide range of metallicity, mass, luminosity and effective temperature with four different sets of convection parameters, A, B, C and D as outlined in Paxton et al. (2019) and Table 1. The metallicity varies from $[\text{Fe}/\text{H}]=-2.0$ dex ($Z=0.00014$) to $[\text{Fe}/\text{H}]=0.0$ dex ($Z=0.013$). The stellar masses vary from $0.5M_{\odot}$ to $0.8M_{\odot}$, while the stellar luminosity varies from $50L_{\odot}$ to $300L_{\odot}$, typical for BL Her stars. Effective temperature is in steps of 50 K inside the instability strip. Non-linear models were computed for 4000 pulsation cycles for periods typical for BL Her stars, i.e. $1 \leq P(\text{days}) \leq 4$. The non-linear models analysed in this study fulfil the condition of full-amplitude stable pulsations, i.e., amplitude of radius variation ΔR , period P and fractional growth rate Γ do not vary by more than 0.01 over the last ~ 100 -cycles of the total 4000-cycle integrations. The total number of BL Her models accepted are 3266 in set A, 2260 in set B, 2632 in set C and 2122 in set D. We have theoretical lightcurves in multiple wavelengths, $UBVRIJHKL\text{LM}$ from the computed non-linear models.

We obtain theoretical multi-wavelength PL , PW and PR relations for these models using the four different sets of convection parameters. We test for the effect of metallicity and convection parameters on the PL and PR relations. We summarise the important results below:

(i) Models computed with sets B and D show statistically similar slopes for PL , PW and PR relations while those with sets A and C exhibit similar slopes for most cases. Sets B and D are the models

computed with radiative cooling; sets A and C are computed without radiative cooling.

(ii) Most empirical relations match well with the theoretical PL , PW and PR relations derived using our BL Her models and over all the four sets of convection parameters.

(iii) An exception to this are the PL relations for BL Her stars in the LMC where PL slopes of the models with sets B and D seem to match better with empirical relations in the HK_S bands.

(iv) We find that the PL slopes from the BL Her models become steeper with increasing wavelengths. The dispersion in the theoretical PL relations for BL Hers decreases significantly moving from optical to infrared wavelengths and becomes statistically similar for wavelengths longer than H -band. We also observe that the models computed using set B have the smallest dispersion in their PL relations in all the bands.

(v) For each set of convection parameters, the effect of metallicity is significant in U and B -bands, and appreciable for bolometric PL relations. It is much weaker in redder bands, consistent with empirical data and previous studies (Matsunaga et al. 2006; Groenewegen & Jurkovic 2017b).

(vi) There is a weak dependence of the PR relations on metallicity with identical coefficient (0.006 ± 0.001) for all 4 sets of convection parameters. The inclusion of the metallicity term does not lead to a significant decrease in dispersion for the relations. This is consistent with the empirical evidence from Burki & Meylan (1986), Balog et al. (1997) and Groenewegen & Jurkovic (2017b).

(vii) The RR Lyrae models from Marconi et al. (2015) exhibit statistically similar PL relations in the $RIJK_S$ bands with those obtained from BL Her models computed using sets A and C while the PR slopes from the RR Lyrae models are statistically similar with the relations from the BL Her models using all four sets of convection parameters.

However, it is important to note here that both the PL and the PR relations derived in this study are at mean light, which averages out the effect of the pulsation cycle. We also note that the comparison among the models computed using different sets of convection parameters has higher precision than when comparing with empirical PL and PW relations. It would seem that observations are not yet sufficiently precise to distinguish fully among the models, although there is a preference for the models that include radiative cooling. It would be interesting to study the effect of different convective parameter sets on the light curve structures of the BL Her models during the pulsation cycle, which we plan to investigate in a future project. The large number of models computed in this study ush-

² In the course of refereeing process of this paper, a new study appeared on ArXiv by Bono et al. (<https://ui.adsabs.harvard.edu/abs/2020arXiv200906985B/abstract>) discussing in more detail the evolutionary properties of T2Cs

Table 10. Comparison of the slopes of the period-luminosity and period-radius relations of the mathematical forms $M_I = a \log(P) + b$ and $\log(R/R_\odot) = \alpha \log(P) + \beta$, respectively for RR Lyrae models from Marconi et al. (2015). N is the total number of models. $|T|$ represents the observed value of the t -statistic, and $p(t)$ gives the probability of acceptance of the null hypothesis (equal slopes). The bold-faced entries indicate that the null hypothesis of the equivalent PL slopes can be rejected.

Band	Source	Slope	Intercept	σ	N	Reference [‡]	Theoretical/ Empirical	$(T , p(t))$ w.r.t. This work			
								Set A	Set B	Set C	Set D
Period-luminosity relation											
R	Z _{all}	-1.756±0.077	-0.114±0.014	0.196	226	M15	Theoretical	(1.19,0.117)	(1.485,0.069)	(0.208,0.418)	(1.882,0.03)
I	Z _{all}	-1.973±0.068	-0.415±0.013	0.175	226	M15	Theoretical	(0.966,0.167)	(1.709,0.044)	(0.561,0.287)	(2.217,0.013)
J	Z _{all}	-2.245±0.06	-0.778±0.011	0.155	226	M15	Theoretical	(0.902,0.184)	(1.769,0.039)	(0.098,0.461)	(1.898,0.029)
H	Z _{all}	-2.206±0.118	-1.043±0.022	0.302	226	M15	Theoretical	(3.056,0.001)	(1.867,0.031)	(2.708,0.003)	(1.889,0.03)
K	Z _{all}	-2.514±0.057	-1.11±0.011	0.147	226	M15	Theoretical	(0.24,0.405)	(2.149,0.016)	(0.507,0.306)	(2.149,0.016)
Period-radius relation											
–	Z _{all}	0.557±0.011	0.871±0.002	0.029	226	M15	Theoretical	(1.622,0.052)	(1.015,0.155)	(1.45,0.074)	(0.596,0.276)

[‡] M15=Marconi et al. (2015)

The PL and PR relations for the RR Lyrae models have been obtained using Table 3 of Marconi et al. (2015). The PL and PR relations for the BL Her models computed in this work using the four sets of convection parameters are available in Table 5 and Table 9, respectively.

ers in the era of large number statistics in the analysis of theoretical models.

ACKNOWLEDGEMENTS

The authors thank the referee for useful comments and suggestions that improved the quality of the manuscript. SD acknowledges the INSPIRE Senior Research Fellowship vide Sanction Order No. DST/INSPIRE Fellowship/2016/IF160068 under the INSPIRE Program from the Department of Science & Technology, Government of India. HPS and SMK thank the Indo-US Science and Technology Forum for funding the Indo-US virtual joint networked centre on “Theoretical analyses of variable star light curves in the era of large surveys”. SD acknowledges the travel support provided by SERB, Government of India vide file number ITS/2019/004781 to attend the RR Lyrae/Cepheid 2019 Conference “Frontiers of Classical Pulsators: Theory and Observations”, USA where this work was initiated. RS is supported by the National Science Center, Poland, Sonata BIS project 2018/30/E/ST9/00598. AB acknowledges research grant #11850410434 from the National Natural Science Foundation of China through the Research Fund for International Young Scientists, a China Post-doctoral General Grant, and the Gruber fellowship 2020 grant sponsored by the Gruber Foundation and the International Astronomical Union. The authors acknowledge the use of High Performance Computing facility Pegasus at IUCAA, Pune and the following software used in this project: MESA r11701 (Paxton et al. 2011, 2013, 2015, 2018, 2019).

DATA AVAILABILITY

The data underlying this article are available in the article and in its online supplementary material.

REFERENCES

Allard F., Hauschildt P. H., 1995, *ApJ*, **445**, 433
 Asplund M., Grevesse N., Sauval A. J., Scott P., 2009, *ARA&A*, **47**, 481
 Balog Z., Vinko J., Kaszas G., 1997, *AJ*, **113**, 1833
 Beaton R. L., et al., 2018, *SSRv*, **214**, 113
 Bessell M. S., Brett J. M., Scholz M., Wood P. R., 1989, *A&AS*, **77**, 1
 Bessell M. S., Brett J. M., Scholz M., Wood P. R., 1991, *A&AS*, **89**, 335
 Bhardwaj A., 2020, *Journal of Astrophysics and Astronomy*, **41**, 23

Bhardwaj A., Kanbur S. M., Singh H. P., Macri L. M., Ngeow C.-C., 2015, *MNRAS*, **447**, 3342
 Bhardwaj A., Kanbur S. M., Macri L. M., Singh H. P., Ngeow C.-C., Wagner-Kaiser R., Sarajedini A., 2016, *AJ*, **151**, 88
 Bhardwaj A., Macri L. M., Rejkuba M., Kanbur S. M., Ngeow C.-C., Singh H. P., 2017a, *AJ*, **153**, 154
 Bhardwaj A., et al., 2017b, *A&A*, **605**, A100
 Bhardwaj A., Rejkuba M., de Grijs R., Herczeg G. J., Singh H. P., Kanbur S., Ngeow C.-C., 2020, *AJ*, **160**, 220
 Bono G., Castellani V., Stellingwerf R. F., 1995, *ApJL*, **445**, L145
 Bono G., Caputo F., Santolamazza P., 1997a, *A&A*, **317**, 171
 Bono G., Caputo F., Cassisi S., Castellani V., Marconi M., 1997b, *ApJ*, **489**, 822
 Bono G., Caputo F., Castellani V., Marconi M., Storm J., Degl’Innocenti S., 2003, *MNRAS*, **344**, 1097
 Braga V. F., Bhardwaj A., Contreras Ramos R., Minniti D., Bono G., de Grijs R., Minniti J. H., Rejkuba M., 2018, *A&A*, **619**, A51
 Braga V. F., et al., 2020, arXiv e-prints, p. arXiv:2010.06368
 Buchler J. R., Moskalik P., 1992, *ApJ*, **391**, 736
 Burki G., Meylan G., 1986, *A&A*, **159**, 261
 Cardelli J. A., Clayton G. C., Mathis J. S., 1989, *ApJ*, **345**, 245
 Catelan M., Pritzl B. J., Smith H. A., 2004, *ApJS*, **154**, 633
 Ciechanowska A., Pietrzyński G., Szewczyk O., Gieren W., Soszyński I., 2010, *AcA*, **60**, 233
 Cioni M. R. L., et al., 2011, *A&A*, **527**, A116
 Clement C. M., et al., 2001, *AJ*, **122**, 2587
 Clementini G., et al., 2016, *A&A*, **595**, A133
 Das S., Bhardwaj A., Kanbur S. M., Singh H. P., Marconi M., 2018, *MNRAS*, **481**, 2000
 Das S., et al., 2020, *MNRAS*, **493**, 29
 Deb S., Singh H. P., 2009, *A&A*, **507**, 1729
 Di Criscienzo M., Caputo F., Marconi M., Cassisi S., 2007, *A&A*, **471**, 893
 Ferguson J. W., Alexander D. R., Allard F., Barman T., Bodnarik J. G., Hauschildt P. H., Heffner-Wong A., Tamanai A., 2005, *ApJ*, **623**, 585
 Fluku M. A., Plez B., The P. S., de Winter D., Westerlund B. E., Steenman H. C., 1994, *A&AS*, **105**, 311
 Gray D. F., 2005, The Observation and Analysis of Stellar Photospheres
 Groenewegen M. A. T., Jurkovic M. I., 2017a, *A&A*, **603**, A70
 Groenewegen M. A. T., Jurkovic M. I., 2017b, *A&A*, **604**, A29
 Groenewegen M. A. T., Udalski A., Bono G., 2008, *A&A*, **481**, 441
 Harris H. C., Wallerstein G., 1984, *AJ*, **89**, 379
 Hinshaw G., et al., 2013, *ApJS*, **208**, 19
 Iglesias C. A., Rogers F. J., 1996, *ApJ*, **464**, 943
 Inno L., et al., 2013, *ApJ*, **764**, 84
 Kudritzki R.-P., Urbaneja M. A., Bresolin F., Przybilla N., Gieren W., Pietrzyński G., 2008, *ApJ*, **681**, 269
 Kuhfuss R., 1986, *A&A*, **160**, 116
 Kurucz R. L., 1970, SAO Special Report, 309
 Lejeune T., Cuisinier F., Buser R., 1998, *A&AS*, **130**, 65

- Macri L. M., Ngeow C.-C., Kanbur S. M., Mahzooni S., Smitka M. T., 2015, *AJ*, **149**, 117
- Madore B. F., 1982, *ApJ*, **253**, 575
- Madore B. F., Freedman W. L., 2012, *ApJ*, **744**, 132
- Majaess D. J., 2010, Journal of the American Association of Variable Star Observers (JAAVSO), **38**, 100
- Mamajek E. E., et al., 2015, arXiv e-prints, p. arXiv:1510.06262
- Manick R., Van Winckel H., Kamath D., Hillen M., Escorza A., 2017, *A&A*, **597**, A129
- Manick R., Van Winckel H., Kamath D., Sekaran S., Kolenberg K., 2018, *A&A*, **618**, A21
- Marconi M., Di Criscienzo M., 2007, *A&A*, **467**, 223
- Marconi M., Bono G., Caputo F., Piersimoni A. M., Pietrinferni A., Stellingwerf R. F., 2011, *ApJ*, **738**, 111
- Marconi M., et al., 2015, *ApJ*, **808**, 50
- Matsunaga N., et al., 2006, *MNRAS*, **370**, 1979
- Matsunaga N., Feast M. W., Menzies J. W., 2009, *MNRAS*, **397**, 933
- Matsunaga N., Feast M. W., Soszyński I., 2011, *MNRAS*, **413**, 223
- Neeley J. R., et al., 2017, *ApJ*, **841**, 84
- Nemec J. M., Nemec A. F. L., Lutz T. E., 1994, *AJ*, **108**, 222
- Ngeow C.-C., Sarkar S., Bhardwaj A., Kanbur S. M., Singh H. P., 2015, *ApJ*, **813**, 57
- Paxton B., Bildsten L., Dotter A., Herwig F., Lesaffre P., Timmes F., 2011, *ApJS*, **192**, 3
- Paxton B., et al., 2013, *ApJS*, **208**, 4
- Paxton B., et al., 2015, *ApJS*, **220**, 15
- Paxton B., et al., 2018, *ApJS*, **234**, 34
- Paxton B., et al., 2019, *ApJS*, **243**, 10
- Ripepi V., et al., 2015, *MNRAS*, **446**, 3034
- Schmidt E. G., Rogalla D., Thacker-Lynn L., 2011, *AJ*, **141**, 53
- Smolec R., 2016, *MNRAS*, **456**, 3475
- Smolec R., Moskalik P., 2008, *AcA*, **58**, 193
- Smolec R., Moskalik P., 2012, *MNRAS*, **426**, 108
- Smolec R., Moskalik P., 2014, *MNRAS*, **441**, 101
- Smolec R., et al., 2012, *MNRAS*, **419**, 2407
- Soszyński I., et al., 2008, *AcA*, **58**, 293
- Soszyński I., et al., 2011, *AcA*, **61**, 285
- Soszyński I., et al., 2014, *AcA*, **64**, 177
- Soszyński I., et al., 2017, *AcA*, **67**, 297
- Soszyński I., et al., 2018, *AcA*, **68**, 89
- Stellingwerf R. F., 1982a, *ApJ*, **262**, 330
- Stellingwerf R. F., 1982b, *ApJ*, **262**, 339
- Wallerstein G., 2002, *PASP*, **114**, 689
- Wallerstein G., Farrell E. M., 2018, *AJ*, **156**, 299
- Welch D. L., 2012, *JAVSO*, **40**, 492
- Wuchterl G., Feuchtinger M. U., 1998, *A&A*, **340**, 419
- Yecko P. A., Kollath Z., Buchler J. R., 1998, *A&A*, **336**, 553

APPENDIX A: *PL* RELATIONS USING DIFFERENT MODEL ATMOSPHERES

MESA provides two sets of pre-processed tables of bolometric corrections (Paxton et al. 2018). The results discussed in this work are using the pre-processed table (BC_1) from Lejeune et al. (1998). To test the impact of the adopted model atmospheres used to transform bolometric light curves to observational bands, we use another pre-processed table (BC_2) which provides a set of blackbody bolometric corrections for the bands $UBVR_cI_c$ over the range $100 \leq T_{\text{eff}}(\text{K}) \leq 50,000$, in steps of 100 K. For the exact same set of models, we compare the slopes of the *PL* relations in the *V* and *I* bands of the mathematical form $\log_{10}(L_{V/I}/L_{\odot}) = a \log(P) + b$ using the two different sets of bolometric corrections, BC_1 and BC_2 . We find the PL_V slopes to be 0.657 ± 0.013 and 0.68 ± 0.012 for 3266 BL Her models in set A, 0.552 ± 0.014 and 0.584 ± 0.013 for 2260 models in set B, 0.6 ± 0.014 and 0.616 ± 0.013 for 2633 models in set C and

0.535 ± 0.014 and 0.559 ± 0.014 for 2122 models in set D using the two different bolometric correction sets BC_1 and BC_2 , respectively. The slopes of the *PL* relations in the *V* band differ by less than 6% when a different model atmosphere incorporated in MESA is adopted. For the *I*-band, the *PL* slopes are 0.825 ± 0.01 and 0.809 ± 0.01 in set A, 0.741 ± 0.011 and 0.728 ± 0.011 in set B, 0.777 ± 0.011 and 0.763 ± 0.011 in set C and 0.724 ± 0.011 and 0.712 ± 0.011 in set D using the different bolometric correction sets BC_1 and BC_2 , respectively. The slopes of the *PL* relations in the *I* band therefore differ by less than 2% when a different model atmosphere is adopted. We find significant variation in *PL* slopes in *U* and *B*-band when the two different bolometric sets are adopted. The effect of different model atmospheres on transformations of bolometric light curves to observational bands reduces as we move to longer wavelengths. We note here that the mean luminosity used for these relations have been obtained from averaging the luminosity of the BL Her model over a pulsation cycle, unlike the mean magnitudes obtained from Fourier fitting as discussed in Section 3.

The reason for adopting the bolometric correction set BC_1 in our present work is that it provides bolometric corrections for the Johnson-Cousins-Class bands $UBVR_cI_c$. BC_2 only provides bolometric corrections for $UBVR_cI_c$. BC_1 defines the bolometric correction as a function of the stellar photosphere; $T_{\text{eff}}(\text{K})$, $\log(g)(\text{cm}^{-2})$, and the metallicity $[M/H]$. Since BC_2 involves blackbody corrections, there is no g or $[M/H]$ dependence. While a more detailed and quantitative comparison using other model atmospheres is important, it is beyond the scope of this paper and we do not anticipate much difference since we are primarily concerned with *PL* relations at mean light. Using the two different bolometric correction sets provided by MESA also suggests that the change in *PL* slopes due to different adopted model transformations is minimal at wavelengths longer than *V*-band. In addition, Paxton et al. (2019) demonstrates that the MESA-RSP code produces stable, multi-wavelength light curve models with reasonable comparison with observations for a wide class of radially pulsating stars. Further, Das et al. (2020) obtained theoretical period-colour relations for a broad spectrum of variable stars, including BL Hers which were in broad agreement with observations.

APPENDIX B: *PLZ* RELATIONS IN THE LOW AND HIGH-METALLICITY REGIMES

To investigate the dependence of *PL* relations on metallicity, we separated models in low-metallicity ($Z = 0.00014, 0.00043, 0.00061, 0.00135$) and high-metallicity ($Z = 0.00424, 0.00834, 0.01300$) regime. The results of *PLZ* relations for the models in the low and high-metallicity regimes using different convection sets are listed in Tables B1 and B2, respectively and discussed in Section 3.2.

Table B1. *PLZ* relations of the mathematical form $M_\lambda = a + b \log(P) + c[\text{Fe}/\text{H}]$ for BL Her models in the low-metallicity regime ($Z = 0.00014, 0.00043, 0.00061, 0.00135$) for different wavelengths using different convective parameter sets.

Band	a	b	c	σ	N
Convection set A					
U	0.305 ± 0.036	-1.217 ± 0.052	0.105 ± 0.022	0.324	1734
B	0.207 ± 0.038	-1.273 ± 0.055	0.027 ± 0.023	0.34	1734
V	-0.163 ± 0.032	-1.605 ± 0.046	-0.01 ± 0.019	0.285	1734
R	-0.39 ± 0.028	-1.827 ± 0.04	-0.015 ± 0.017	0.25	1734
I	-0.611 ± 0.024	-2.024 ± 0.035	-0.009 ± 0.015	0.22	1734
J	-0.93 ± 0.021	-2.268 ± 0.03	-0.003 ± 0.013	0.189	1734
H	-1.179 ± 0.018	-2.543 ± 0.026	0.005 ± 0.011	0.159	1734
K	-1.134 ± 0.018	-2.499 ± 0.026	0.005 ± 0.011	0.163	1734
L	-1.239 ± 0.017	-2.574 ± 0.025	0.006 ± 0.01	0.157	1734
L'	-1.242 ± 0.017	-2.576 ± 0.025	0.007 ± 0.01	0.157	1734
M	-1.482 ± 0.015	-2.842 ± 0.022	0.018 ± 0.009	0.14	1734
Bolometric	-0.176 ± 0.028	-1.806 ± 0.041	0.022 ± 0.017	0.253	1734
Convection set B					
U	0.344 ± 0.035	-0.958 ± 0.049	0.117 ± 0.022	0.271	1217
B	0.245 ± 0.037	-1.006 ± 0.051	0.035 ± 0.023	0.286	1217
V	-0.14 ± 0.032	-1.372 ± 0.044	-0.005 ± 0.02	0.246	1217
R	-0.375 ± 0.028	-1.616 ± 0.039	-0.01 ± 0.017	0.22	1217
I	-0.605 ± 0.026	-1.833 ± 0.035	-0.005 ± 0.016	0.198	1217
J	-0.935 ± 0.023	-2.09 ± 0.031	0.002 ± 0.014	0.174	1217
H	-1.195 ± 0.02	-2.386 ± 0.027	0.009 ± 0.012	0.153	1217
K	-1.148 ± 0.02	-2.338 ± 0.028	0.009 ± 0.012	0.156	1217
L	-1.255 ± 0.02	-2.419 ± 0.027	0.01 ± 0.012	0.152	1217
L'	-1.258 ± 0.02	-2.421 ± 0.027	0.011 ± 0.012	0.152	1217
M	-1.508 ± 0.018	-2.709 ± 0.025	0.022 ± 0.011	0.14	1217
Bolometric	-0.162 ± 0.029	-1.58 ± 0.04	0.027 ± 0.018	0.222	1217
Convection set C					
U	0.414 ± 0.041	-0.792 ± 0.056	0.129 ± 0.025	0.318	1292
B	0.327 ± 0.041	-0.935 ± 0.057	0.039 ± 0.025	0.323	1292
V	-0.077 ± 0.035	-1.362 ± 0.048	-0.008 ± 0.021	0.273	1292
R	-0.328 ± 0.031	-1.618 ± 0.043	-0.014 ± 0.019	0.242	1292
I	-0.57 ± 0.028	-1.843 ± 0.038	-0.009 ± 0.017	0.217	1292
J	-0.91 ± 0.024	-2.142 ± 0.033	-0.005 ± 0.015	0.188	1292
H	-1.184 ± 0.02	-2.472 ± 0.028	0.002 ± 0.012	0.16	1292
K	-1.136 ± 0.021	-2.415 ± 0.029	0.002 ± 0.013	0.164	1292
L	-1.246 ± 0.02	-2.506 ± 0.028	0.003 ± 0.012	0.158	1292
L'	-1.248 ± 0.02	-2.509 ± 0.028	0.004 ± 0.012	0.157	1292
M	-1.507 ± 0.018	-2.823 ± 0.025	0.017 ± 0.011	0.14	1292
Bolometric	-0.111 ± 0.031	-1.606 ± 0.043	0.024 ± 0.019	0.245	1292
Convection set D					
U	0.429 ± 0.038	-0.762 ± 0.05	0.127 ± 0.024	0.28	1094
B	0.334 ± 0.04	-0.87 ± 0.052	0.033 ± 0.025	0.29	1094
V	-0.075 ± 0.034	-1.28 ± 0.045	-0.01 ± 0.021	0.251	1094
R	-0.327 ± 0.031	-1.536 ± 0.04	-0.015 ± 0.019	0.226	1094
I	-0.569 ± 0.028	-1.76 ± 0.037	-0.008 ± 0.017	0.205	1094
J	-0.912 ± 0.025	-2.047 ± 0.033	-0.001 ± 0.016	0.183	1094
H	-1.188 ± 0.022	-2.369 ± 0.029	0.008 ± 0.014	0.161	1094
K	-1.139 ± 0.023	-2.314 ± 0.029	0.008 ± 0.014	0.164	1094
L	-1.25 ± 0.022	-2.402 ± 0.029	0.01 ± 0.014	0.16	1094
L'	-1.252 ± 0.022	-2.405 ± 0.029	0.011 ± 0.014	0.16	1094
M	-1.513 ± 0.02	-2.715 ± 0.026	0.026 ± 0.012	0.146	1094
Bolometric	-0.109 ± 0.031	-1.511 ± 0.041	0.023 ± 0.019	0.227	1094

Table B2. *PLZ* relations of the mathematical form $M_\lambda = a + b \log(P) + c[\text{Fe}/\text{H}]$ for BL Her models in the high-metallicity regime ($Z = 0.00424, 0.00834, 0.01300$) for different wavelengths using different convective parameter sets.

Band	a	b	c	σ	N
Convection set A					
U	0.432 ± 0.026	-0.816 ± 0.062	0.442 ± 0.048	0.382	1532
B	0.288 ± 0.024	-1.187 ± 0.057	0.173 ± 0.045	0.353	1532
V	-0.118 ± 0.019	-1.642 ± 0.046	0.043 ± 0.036	0.282	1532
R	-0.358 ± 0.017	-1.873 ± 0.04	0.015 ± 0.031	0.245	1532
I	-0.579 ± 0.015	-2.066 ± 0.035	0.027 ± 0.027	0.217	1532
J	-0.89 ± 0.012	-2.347 ± 0.03	0.025 ± 0.023	0.182	1532
H	-1.135 ± 0.01	-2.621 ± 0.025	0.039 ± 0.019	0.153	1532
K	-1.086 ± 0.011	-2.583 ± 0.025	0.041 ± 0.02	0.157	1532
L	-1.192 ± 0.01	-2.652 ± 0.025	0.044 ± 0.019	0.152	1532
L'	-1.193 ± 0.01	-2.652 ± 0.025	0.048 ± 0.019	0.152	1532
M	-1.427 ± 0.01	-2.833 ± 0.023	0.103 ± 0.018	0.14	1532
Bolometric	-0.108 ± 0.017	-1.864 ± 0.04	0.092 ± 0.031	0.248	1532
Convection set B					
U	0.411 ± 0.027	-0.428 ± 0.069	0.385 ± 0.053	0.35	1043
B	0.269 ± 0.025	-0.847 ± 0.064	0.1 ± 0.05	0.328	1043
V	-0.141 ± 0.02	-1.372 ± 0.052	-0.02 ± 0.04	0.267	1043
R	-0.383 ± 0.018	-1.638 ± 0.046	-0.041 ± 0.036	0.235	1043
I	-0.606 ± 0.016	-1.856 ± 0.041	-0.021 ± 0.032	0.21	1043
J	-0.921 ± 0.014	-2.175 ± 0.035	-0.02 ± 0.027	0.18	1043
H	-1.168 ± 0.012	-2.488 ± 0.03	0.002 ± 0.024	0.155	1043
K	-1.119 ± 0.012	-2.445 ± 0.031	0.002 ± 0.024	0.158	1043
L	-1.225 ± 0.012	-2.522 ± 0.03	0.008 ± 0.023	0.153	1043
L'	-1.227 ± 0.012	-2.522 ± 0.03	0.011 ± 0.023	0.154	1043
M	-1.462 ± 0.011	-2.727 ± 0.028	0.076 ± 0.022	0.143	1043
Bolometric	-0.134 ± 0.018	-1.622 ± 0.046	0.032 ± 0.036	0.237	1043
Convection set C					
U	0.605 ± 0.031	-0.553 ± 0.074	0.46 ± 0.06	0.438	1340
B	0.465 ± 0.027	-1.097 ± 0.064	0.143 ± 0.052	0.38	1340
V	0.012 ± 0.021	-1.602 ± 0.05	0.009 ± 0.041	0.3	1340
R	-0.261 ± 0.019	-1.828 ± 0.044	-0.016 ± 0.036	0.263	1340
I	-0.509 ± 0.017	-2.008 ± 0.039	0.003 ± 0.032	0.234	1340
J	-0.849 ± 0.014	-2.324 ± 0.032	-0.003 ± 0.026	0.192	1340
H	-1.127 ± 0.011	-2.601 ± 0.027	0.02 ± 0.022	0.16	1340
K	-1.074 ± 0.012	-2.563 ± 0.027	0.019 ± 0.022	0.163	1340
L	-1.186 ± 0.011	-2.634 ± 0.026	0.024 ± 0.021	0.158	1340
L'	-1.187 ± 0.011	-2.635 ± 0.027	0.028 ± 0.021	0.158	1340
M	-1.447 ± 0.01	-2.796 ± 0.024	0.101 ± 0.02	0.145	1340
Bolometric	-0.004 ± 0.019	-1.843 ± 0.044	0.06 ± 0.036	0.262	1340
Convection set D					
U	0.545 ± 0.034	-0.275 ± 0.083	0.399 ± 0.066	0.428	1028
B	0.412 ± 0.03	-0.844 ± 0.073	0.078 ± 0.058	0.375	1028
V	-0.028 ± 0.023	-1.403 ± 0.058	-0.043 ± 0.046	0.297	1028
R	-0.294 ± 0.02	-1.659 ± 0.05	-0.06 ± 0.04	0.26	1028
I	-0.536 ± 0.018	-1.862 ± 0.045	-0.034 ± 0.036	0.231	1028
J	-0.87 ± 0.015	-2.208 ± 0.037	-0.034 ± 0.03	0.191	1028
H	-1.14 ± 0.013	-2.519 ± 0.031	-0.003 ± 0.025	0.16	1028
K	-1.089 ± 0.013	-2.477 ± 0.032	-0.005 ± 0.025	0.164	1028
L	-1.199 ± 0.012	-2.554 ± 0.031	0.003 ± 0.025	0.158	1028
L'	-1.2 ± 0.012	-2.555 ± 0.031	0.006 ± 0.025	0.158	1028
M	-1.454 ± 0.012	-2.739 ± 0.028	0.088 ± 0.023	0.147	1028
Bolometric	-0.038 ± 0.02	-1.667 ± 0.05	0.011 ± 0.04	0.26	1028